Eur. Phys. J. C (2023) 83:1081
https://doi.org/10.1140/epjc/s10052-023-12024-6

THE EUROPEAN PHYSICAL JOURNAL C

Regular Article - Experimental Physics

Performance of the reconstruction of large impact parameter tracks in the inner detector of ATLAS

ATLAS Collaboration[*]

CERN, 1211 Geneva 23, Switzerland

Received: 26 April 2023 / Accepted: 10 September 2023

Abstract Searches for long-lived particles (LLPs) are among the most promising avenues for discovering physics beyond the Standard Model at the Large Hadron Collider (LHC). However, displaced signatures are notoriously difficult to identify due to their ability to evade standard object reconstruction strategies. In particular, the ATLAS track reconstruction applies strict pointing requirements which limit sensitivity to charged particles originating far from the primary interaction point. To recover efficiency for LLPs decaying within the tracking detector volume, the ATLAS Collaboration employs a dedicated large-radius tracking (LRT) pass with loosened pointing requirements. During Run 2 of the LHC, the LRT implementation produced many incorrectly reconstructed tracks and was therefore only deployed in small subsets of events. In preparation for LHC Run 3, ATLAS has significantly improved both standard and large-radius track reconstruction performance, allowing for LRT to run in all events. This development greatly expands the potential phase-space of LLP searches and streamlines LLP analysis workflows. This paper will highlight the above achievement and report on the readiness of the ATLAS detector for track-based LLP searches in Run 3.

Contents

1 Introduction

One promising way to search for physics beyond the Standard Model (BSM) is at the energy frontier, probing energies comparable to those present very shortly after the Big Bang. Thus far, the overwhelming majority of searches for new physics at CERN's Large Hadron Collider (LHC) [1] have been performed under the assumption that the BSM particles decay promptly, i.e., very close to the proton–proton (pp) interaction point (IP). However, BSM theories often predict the existence of particles with relatively long proper lifetimes (τ) [2–4]. For particles moving close to the speed of light (c), this can lead to macroscopic displacements between the production and decay points of a new long-lived particle (LLP). When τ is of $\mathcal{O}(0.1) - \mathcal{O}(10)$ ns, the decay will predominantly take place within the ATLAS inner detector (ID). Searches for LLPs have been performed by the ATLAS Collaboration in the past [5–12], reconstructing explicitly their decay vertices within the ATLAS ID volume.

In order to reconstruct the trajectories of charged particles, ATLAS uses the ID tracking system to provide efficient, robust and precise position measurements of charged particles as they traverse the detector. The energy deposits from charged particles (hits) recorded in individual detector elements of the ID are used to reconstruct their trajectories (tracks) and estimate the associated track parameters. The standard track reconstruction pass (primary pass) in ATLAS is optimised for particles that originate at the primary IP,

[*] e-mail: atlas.publications@cern.ch

Published online: 27 November 2023

which are referred to as primary particles. Here, a pass is defined as a single track-finding iteration. In the primary pass, candidate tracks are required to originate close to the IP thus keeping the computation time reasonable while still being highly efficient in reconstructing primary particles. Several dedicated algorithms are then used to reconstruct a limited set of specific topologies of displaced decays from well-known Standard Model (SM) particles, such as from photon conversions and b-hadron decays. However, the primary pass does not efficiently reconstruct charged particles from LLP decays that are displaced by more than 5 mm from the IP in the transverse plane, except for specific cases involving photon conversions. Consequently, an additional dedicated track reconstruction pass, the so-called *large-radius tracking pass* (LRT pass), is required to extend the ATLAS sensitivity to a larger particle lifetime range.

For the LHC Run 2 data-taking period (2015-2018) the LRT pass was solely optimised for high signal efficiency, resulting in approximately twice the computational time per event compared to the primary pass [13]. To accommodate this increased processing time, the LRT pass was only applied to approximately 10% of the events recorded by the ATLAS detector in a dedicated data stream processed whenever computing resources were available. For the LHC Run 3 (2022-2025) data-taking, the average number of simultaneous pp collisions per bunch crossing, $\langle\mu\rangle$, is expected to increase to well over 50 from Run 2 values that ranged between 20 and 40. As $\langle\mu\rangle$ increases, so does the number of potential hit combinations and therefore the computational time of the LRT pass. In preparation for these challenging Run 3 conditions, the LRT pass was updated, significantly reducing the computation time for the track reconstruction of LLP signatures and drastically reducing the number of so-called fake tracks due to random hit combinations. In parallel, the computation time of the primary pass was improved by a factor of two [14]. As a consequence of these improvements, a full integration of the LRT reconstruction for LLP signatures into the standard ATLAS event reconstruction chain was achieved. This will enable all ID-based LLP searches, including new searches using Run 2 data,[1] to use common data streams, eliminating the need to use a dedicated processing workflow for this application used in Run 2. A schematic diagram illustrating both event reconstruction workflows is shown in Fig. 1.

This paper describes the "offline" reconstruction performance of this dedicated LRT pass. The updated LRT track reconstruction was also implemented in the "online"[2] reconstruction chain leading to similar performance improvements and consequently new LLP trigger algorithms for Run 3. The "online" performance is out of the scope of this paper. The paper is organised as follows: a brief description of the ATLAS detector is given in Sect. 2. Section 3 lists the Monte Carlo (MC) simulation and data samples used to determine the performance. Section 4 presents the formalism of the ATLAS track reconstruction and the dedicated LRT pass. Detailed performance results based both on simulation and data are presented in Sects. 5 and 6, respectively. Concluding remarks are made in Sect. 7.

2 The ATLAS detector

The ATLAS detector [16] at the LHC is a multipurpose particle detector with a forward-backward symmetric cylindrical geometry that covers nearly the entire solid angle around the collision point.[3] It is composed of the ID, electromagnetic and hadronic calorimeters, and a muon spectrometer. Lead/liquid-argon sampling calorimeters provide electromagnetic energy measurements with high granularity and a hadronic (steel/scintillator-tile) calorimeter covers the central pseudorapidity range up to $|\eta| < 1.7$. The end-cap and forward regions are instrumented with liquid-argon calorimeters for both the electromagnetic and hadronic energy measurements up to $|\eta| = 4.9$. The outer part of the detector consists of a muon spectrometer with high-precision tracking chambers for coverage up to $|\eta| = 2.7$, fast detectors for triggering over $|\eta| < 2.4$, and three large superconducting toroid magnets with eight coils each. The ATLAS detector has a two-level trigger system to select events for offline analysis [17]. An extensive software suite [18] is used in data simulation, in the reconstruction and analysis of real and simulated data, in detector operations, and in the trigger and data acquisition systems of the experiment.

2.1 ATLAS inner detector

The ATLAS ID [19,20] is composed of three subdetectors utilising three technologies: silicon pixel detectors, silicon strip detectors and straw drift tubes, all surrounded by a thin superconducting solenoid providing a 2T axial magnetic field. The ID is designed to efficiently reconstruct charged particles within a pseudorapidity range of $|\eta| < 2.5$. Fig-

[1] A full re-processing of all events recorded by ATLAS during the LHC Run 2 was completed using the updated workflow allowing a seamless combination of datasets in the future.

[2] Here, "online" refers to services and reconstruction algorithms that run during real-time data-taking at ATLAS.

[3] The ATLAS reference frame is a right-handed Cartesian coordinate system, where the origin is at the nominal pp interaction point, corresponding to the centre of the detector. The positive x-axis points to the centre of the LHC ring, the positive y-axis points upwards and the z-axis points along the beam direction. Cylindrical coordinates (r, ϕ) are used in the transverse plane, ϕ being the azimuthal angle around the beam pipe. The pseudorapidity is defined in terms of the polar angle θ as $\eta = -\ln\tan(\theta/2)$. Angular distance is measured in units of $\Delta R \equiv \sqrt{(\Delta\eta)^2 + (\Delta\phi)^2}$.

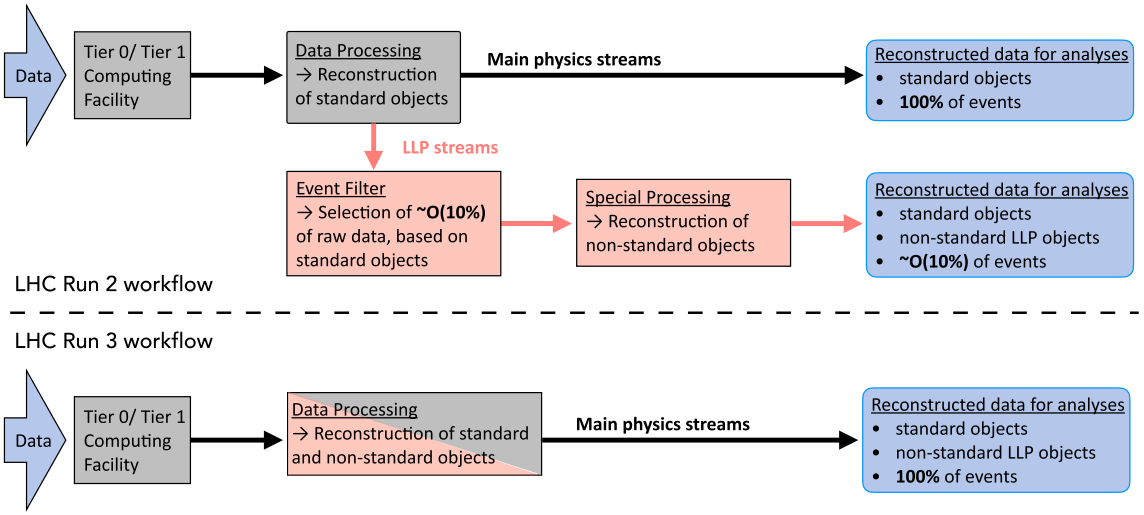

Fig. 1 Schematic diagram illustrating the LHC Run 2 (top) and improved Run 3 (bottom) event reconstruction workflows for the main physics and LLP streams. ATLAS defines a hierarchical "Tier" structure for computing infrastructure, where the Tier 0 farm at CERN is used for initial reconstruction of the recorded data and later data reprocessing proceeds primarily on the eleven Tier 1 sites [15]

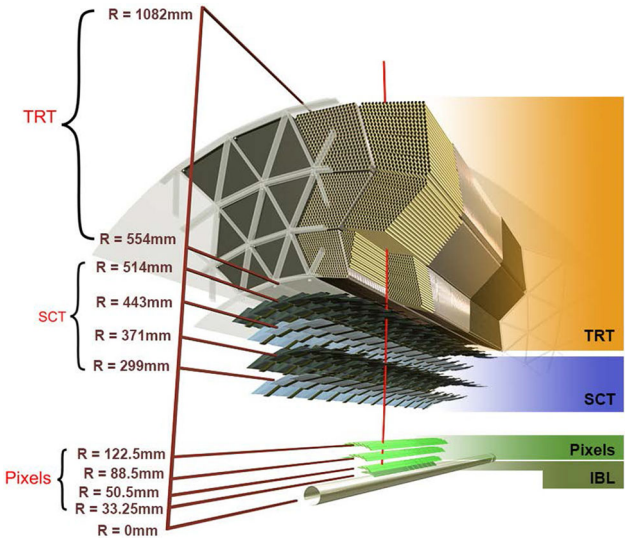

Fig. 2 A 3D visualisation of the structure of the barrel of the ID. The beam-pipe, the IBL, the Pixel layers, the four cylindrical layers of the SCT and the 72 straw layers of the TRT are shown

ure 2 shows a schematic view of the ID barrel region and a list of the main detector characteristics is provided in Table 1. The material distribution inside the ID has been studied in data through use of hadronic interactions and photon conversion vertices [21]. During the second LHC data taking run with pp collisions at a centre-of-mass energy $\sqrt{s} = 13$ TeV, the ID collected data with an efficiency greater than 99% [15].

The innermost part of the ID consists of a high-granularity silicon pixel detector that includes the insertable B-layer (IBL) [22,23], a tracking layer added for Run 2 which is closest to the beam line and designed to improve the precision and robustness of track reconstruction. The IBL comprises 280 silicon pixel modules arranged on 14 azimuthal carbon fibre staves surrounding the beam pipe at an average radius of 33.25 mm. The remainder of the Pixel detector [19,20] is made of 1744 silicon pixel modules arranged in three barrel layers and two end caps with three disks each. In order to simplify the notation throughout the remainder of this paper, the term *Pixel* will be used to refer to the entire subdetector utilising the silicon pixel detectors, including IBL.

The Semiconductor Tracker (SCT) [24] contains 4088 silicon strip modules. They are arranged in four barrel layers and two end caps with nine disks each. Each module consists of two pairs of single sided strip sensors glued back-to-back (axial and stereo sides) with a 40mrad angle.

The Transition Radiation Tracker (TRT) [25] is the outermost subdetector of the ID and extends track reconstruction radially outwards to a radius of 1082 mm. It is made of 350848 gas-filled straw tubes of 4 mm diameter. The tubes are arranged in 96 barrel modules in 3 layers (32 modules per layer) and 40 disks in each end-cap. Drift time measurements from the straw tubes are translated into calibrated drift circles. These allow the TRT to add an average of about 30 two-dimensional additional points to reconstructed tracks that have $|\eta| < 2.0$.

The expected hit resolutions and layer positions for each subdetector are summarised in Table 1. In order to efficiently reconstruct tracks from LLP decays inside the ID, the radial position of the respective detection layers is crucial. In this context, LRT has good efficiency up to radius of approximately 300 mm, which corresponds to the radii of the first SCT barrel layer. Particle decays beyond 300 mm generally

Table 1 Summary of the main characteristics of the ID subdetectors. The intrinsic resolution of the Pixel sensors are reported along r–ϕ and z, while for SCT and TRT only the resolution along $r-\phi$ is given

Subdetector	Intrinsic resolution [μm]	Barrel layer radii [mm]
Pixel (IBL)	8×40	33.2
Pixel (non IBL)	10×115	50.5, 88.5, 122.5
SCT	17	299, 371, 443, 514
TRT	130	from 554 to 1082

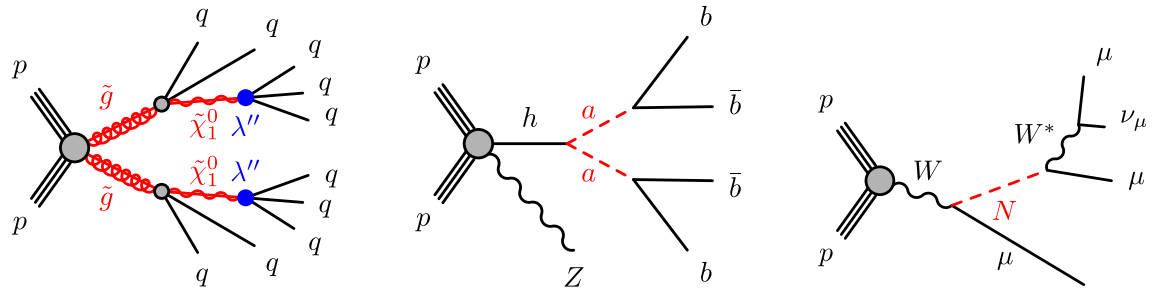

(a) Long-lived neutralino (b) Higgs portal (c) Heavy neutral lepton

Fig. 3 Representative Feynman diagrams of models used to characterise the performance of the LRT algorithm

do not create a sufficient number of silicon hits to be reliably reconstructed.

3 Simulation and data samples

To analyze the performance of the LRT pass on BSM physics of interest, three representative BSM scenarios are studied. Each of these scenarios are characterised by the production of long-lived neutral particles which subsequently decay into charged SM particles. These signatures have a high probability of producing charged particles in the ID, and therefore to produce a high number of displaced tracks. The choice of the three representative benchmark scenarios is driven by the different decay chains that characterise the event topology and impact the kinematics.

The first signal is a Supersymmetric model where pair production of gluinos subsequently cascade to a final state with a large number of quarks. In the sample used, each gluino ($\tilde{g}$) decays into two quarks and a neutralino ($\tilde{\chi}_1^0$), which, in turn, decays into three quarks via the R-parity violating coupling λ'' [26–32]. Hence, from the gluino pair production the final state at tree level consists of ten quarks (where $q = u, d, s, c$). A sketch of the physics process is shown in Fig. 3a. The mass of the gluino and neutralino are set to 1.6 TeV and 50 GeV respectively and the neutralino coupling is set such that the proper decay length $c\tau = 300$ mm. This set of parameters allows to study the performance of the track reconstruction algorithm on high-multiplicity hadronic tracks with high momentum originated from the displaced vertex. The signal samples are generated at leading-order (LO) accuracy with up to two additional partons in the matrix element using the `MadGraph5_aMC@NLO v2.3.3` event generator [33] interfaced with `Pythia 8.212` [34], using the `A14` [35] tune for the underlying event. The parton luminosities are provided by the `NNPDF2.3LO` PDF set [36].

The second signal explored is an exotic Higgs boson decay inspired by hidden-sector models with a Higgs portal [37–40]. In this model, a Higgs boson h produced in association with a Z boson decays into two electrically neutral pseudoscalar particles (a) which each decay into a pair of b quarks, as shown in Fig. 3b. In the sample studied, the mean proper decay length and mass of the a boson are set to 100 mm and 55 GeV respectively, such that a sizeable fraction of displaced vertices formed by the a decays are produced inside the ID. The $h \to aa \to b\bar{b}b\bar{b}$ decay forms displaced vertices with fewer charged particles and lower track momenta than the long-lived neutralino signal. The signal tests the tracking algorithms in an environment with lower track density. Samples of simulated events with a Higgs boson produced in association with a leptonically-decaying Z boson are generated using `Powheg Box v2` [41] at next-to-leading order (NLO) with up to one additional jet. The interface with the `GoSam` package [42] provides one-loop amplitude corrections. The `PDF4LHC15nlo` PDF set [43] is used. The decay of the Higgs boson into pseudoscalars and their subsequent decay into b-quarks are simulated with `Pythia 8.212`. The latter is also used to simulate the parton showering and hadronisation, as well as underlying event, with the `AZNLO CTEQ6L1` set [44] of tuned parameters.

The last signal considered is a displaced heavy neutral lepton (HNL) [45–48], since it can isolate the behaviour of LRT for displaced muon tracks. This signal is motivated by theories in which SM left-chiral neutrinos mix with a theoretical

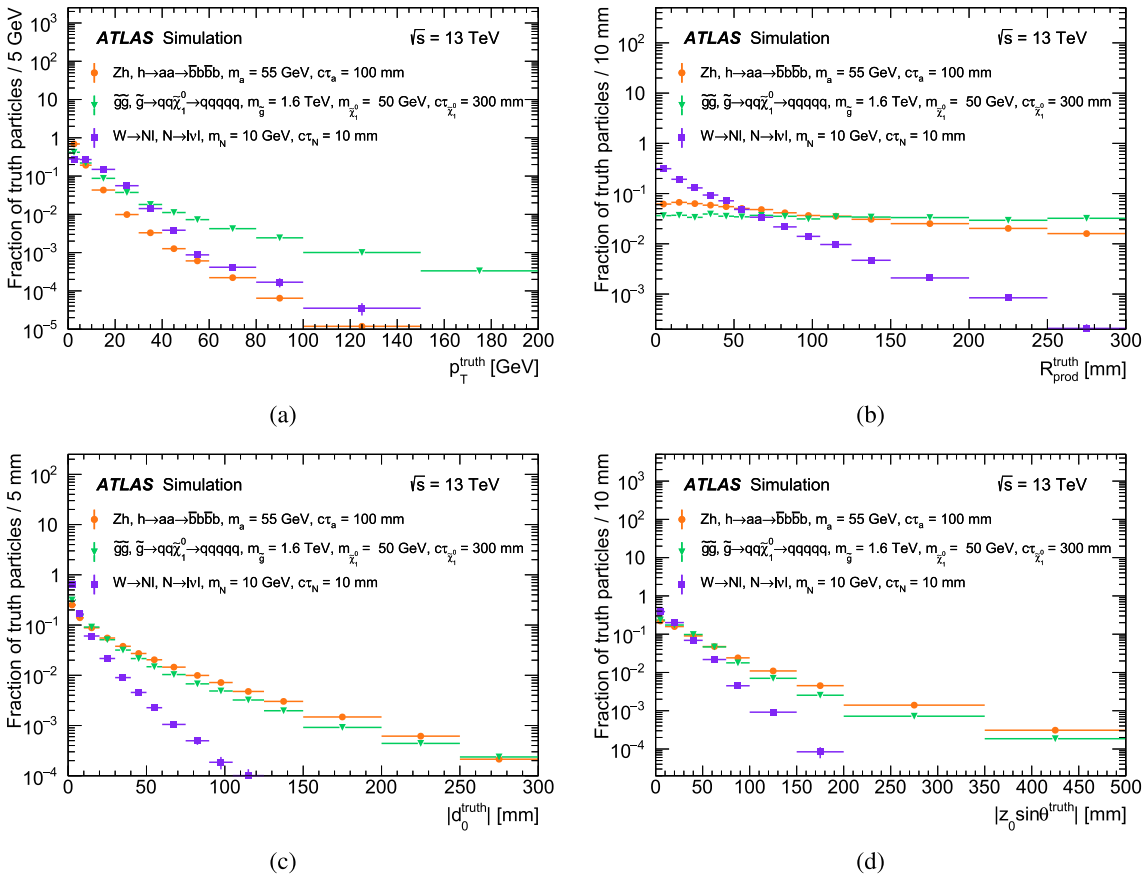

Fig. 4 Comparison of the (**a**) $p_{\mathrm{T}}^{\mathrm{truth}}$, (**b**) $R_{\mathrm{prod}}^{\mathrm{truth}}$, (**c**) $|d_0^{\mathrm{truth}}|$ and (**d**) $|z_0 \sin\theta^{\mathrm{truth}}|$ distributions of the stable charged decay products of the long-lived neutralino, Higgs portal and heavy neutral lepton signal samples

massive right-chiral counterpart providing an explanation to the origin of the neutrino mass. The small mixing between the HNL (N) and the neutrinos result in a long proper lifetime of the BSM particle. In this particular signal a W boson decays into a muon and a neutrino, that mixes with the N. The latter subsequently decays into two muons and a muon neutrino via an off-shell W or Z boson. A representation of one of the possible Feynman diagrams of the signal is shown in Fig. 3c. The mean proper decay length and mass of the N are 10 mm and 10 GeV respectively, such that the displaced leptons are produced in the ID. Differing from the two aforementioned signals, this signature allows to study the performance of the tracking algorithms for displaced isolated muon tracks in low-track multiplicity vertices. `Pythia 8.212` is adopted to generate the events with the `A14` [35] set of tuned parameters and the `NNPDF2.3LO` PDF set [36].

The three signal models vary significantly in terms of the charged particle multiplicity in displaced vertices, as illustrated in Fig. 3. In particular, the long-lived neutralino has the highest track multiplicity and the HNL has the lowest. Truth particles (particles generated in the MC simulation) are subject to fiducial selection criteria that require the particle to be from a LLP decay within $R_{\mathrm{prod}} < 400$ mm, and be stable and charged. Additional selections are imposed on the $p_{\mathrm{T}} > 1.2$ GeV and $|\eta| < 2.5$ of the truth particles. To further highlight the different event topologies of the three new physics signatures, a comparison of the kinematic distributions of charged truth particles is shown in Fig. 4 as a function the transverse momentum ($p_{\mathrm{T}}^{\mathrm{truth}}$), the production radius[4] ($R_{\mathrm{prod}}^{\mathrm{truth}}$), the transverse impact parameter (d_0^{truth}), and the longitudinal impact parameter times $\sin\theta$ ($z_0 \sin\theta^{\mathrm{truth}}$). All truth quantities use the simulated beam spot as reference.

A data sample recorded during 2018 is used to compare the tracking performance between simulation and data. These are selected from the "zero bias" data stream collected using an unbiased random trigger which fires on the bunch crossing occurring one LHC revolution after a low-threshold calorimeter-based trigger [49]. This ensures that data are collected with equivalent beam conditions to the rest of the

[4] The production radius is defined as the radial distance in the transverse plane where the particle is produced, measured with respect to the detector origin.

standard physics data. The total number of recorded events is 25, 485, 193. Selected data are compared to a simulation sample of inelastic pp collisions generated with EPOS [50] to describe processes with leading jet $p_{\mathrm{T}} < 35$ GeV and with Pythia 8.244 [34] for events with a leading jet $p_{\mathrm{T}} > 35$ GeV, based on the NNPDF2.3LO PDF [36], using the A3 [51] tune.

Additional samples are simulated using modified detector geometries to assess the impact of the modeling of the inner detector material on the track reconstruction efficiency. These samples include one with an overall 5% scaling of the passive material in ID, one with a 10% scaling of the IBL, and one with a 25% scaling to the pixel services. A fourth variation is simulated using the QGSP_BIC physics list instead of the nominal FTFP_BERT physics list [52] to quantify the impact of the choice of parameters in the GEANT4 simulation.

All data and simulation samples were reprocessed using the Run 3 reconstruction software [14]. Simulation samples are generated with a flat $\langle\mu\rangle$ profile between 0 and 80. In the case of the comparison with data events, they are reweighted to match the distribution of $\langle\mu\rangle$ in data with a mean value of 34.

4 Track reconstruction

The primary pass in ATLAS is centred on one *inside-out* track reconstruction sequence. This sequence is seeded in the silicon detectors and additional measurements are added throughout the ID along the seed trajectory. In order to improve the reconstruction efficiency for photon conversion events within the ID, an additional *outside-in* track reconstruction sequence is performed within so-called regions of interest (ROI). The LRT is performed as a third tracking sequence, following the primary *inside-out* and *outside-in* tracking.

4.1 Primary tracking

The primary track reconstruction algorithm first looks for track seeds in the Pixel and SCT detectors. A seed is a collection of three space points (SP)[5] each from a unique layer of the Pixel or SCT detectors, requiring a minimum spatial separation between all three points. Track seeds are labelled by their middle SP and can only be built from three Pixel or three SCT SPs, but not combinations of SPs from both detectors. The compatibility of a fourth SP in a different layer is used to further confirm that the seed is likely to originate from a charged particle. In this step, a new seed is formed replacing the outer-most SP of the initial seed and the curvature of the new seed is compared for compatibility to the original one. A confirmed seed is given high priority as a promising candidate in the ranked list of seeds. This list is composed of all track seeds passing certain quality criteria, including a PT and impact parameter selection (see Table 2 for details). Here and throughout the rest of the paper, the beam spot [53] is used as a reference for all impact parameter calculations.

The seeds are used as a starting point to find track candidates using a combinatorial Kalman filter [54,55]. This pattern recognition step combines both measurement association and track fitting in both directions of the initial seed. Track candidates are then processed by the so-called ambiguity-solving algorithm [56]. The ambiguity solver is responsible for deciding the final hit assignments in the case of multiple track candidates using the same hit. Track candidates are evaluated based on various requirements including track p_{T}, number of hits, number of shared hits, and holes.[6] This step removes low-quality candidates resulting in a collection of high-quality tracks from the track candidates formed within the pattern recognition stage.

Within the ambiguity solver, track candidates are re-fit using a global χ^2 method to obtain the final high-precision track parameter estimate. This method is based on the Newton–Raphson method and uses an iterative approach to find the best fit to a set of measurements of a track left in the detector by a charged particle traversing active detector elements. The quality of the fit is characterised by track χ^2, determined from the distances between the hits in the detector, which constitutes the track measurements, and the fitted track. The track fit accounts for the effects of multiple Coulomb scattering of the particle with the detector components. A detailed description can be found in Ref. [57]. An extension of the track into the TRT subdetector is attempted, with a re-fit of the entire track being performed in case of a successful extension to profit from the additional measurements.

The *outside-in* sequence is performed using the detector hits not already assigned to tracks from the *inside-out* reconstruction. The ROIs are determined by deposits in the electromagnetic calorimeter with transverse energy $E_{\mathrm{T}} > 6$ GeV. This second sequence uses segments of hits in the TRT that are spatially compatible with the ROI to find 2-SP SCT track seeds, that are extended inwards into track candidates using the same procedure as for the primary pass but with reduced hit criteria. A dedicated ambiguity resolution step is performed among all track candidates in the second pass and

[5] A SP is defined as a measurement in the Pixel detector or the combination of axial and stereo layers of the SCT detectors.

[6] Hits are defined as measurements from the Pixel, SCT, or TRT detectors; a hole is defined as a missing hit on an active module where one was expected based on the particle trajectory; only silicon detectors are considered in the calculation of holes. Shared hits are those which are used in multiple reconstructed tracks (strong indicator of incorrect assignments). Modules are the individual silicon sensors.

a re-fit of the resulting tracks including their TRT extension completes the *outside-in* sequence.

The resulting tracks, from both *inside-out* and *outside-in* sequences, form the final collection of reconstructed primary tracks. The trajectory of these tracks is parameterised by a set of five parameters: d_0, z_0, ϕ_0, θ_0, q/p, where d_0 and z_0 are the transverse and longitudinal impact parameters and ϕ_0 and θ_0 the azimuthal and polar angles of the track, all defined at the point of closest approach to the z-axis of the reference frame [57]. The ratio q/p is the inverse of the particle momentum (p) multiplied by its charge (q).

4.2 Large-radius tracking

The LRT sequence is executed after the primary tracking iteration using exclusively the detector hits not already assigned to primary tracks, ensuring a completely independent collection of tracks. It adopts the same logic as the primary *inside-out* tracking iteration but it is specifically optimised for LLP signatures. As mentioned previously, a legacy implementation of LRT was used during the LHC Run 2 data-taking that was optimised for high LLP signal-track reconstruction efficiency at the expense of a very large fake track rate (see Sect. 4.3 for a detailed definition). These choices resulted in a computationally-expensive algorithm that could only be operated on a small fraction of events recorded by the ATLAS experiment in a dedicated stream. In preparation for LHC Run 3 the LRT sequence was reoptimised to substantially reduce the required computational resources per event, and consequently integrate LRT as a third common tracking sequence that is executed for each event within the updated default ATLAS event reconstruction chain.

This section gives a detailed description of the reoptimised LRT sequence and the implemented changes. Two guiding principles were followed during the optimisation to substantially speed up the processing time and reduce disk usage per event: (1) identify and terminate the track reconstruction for fake candidate tracks as early as possible within the reconstruction sequence, and (2) significantly reduce the overall number of falsely reconstructed tracks while maintaining high signal track reconstruction efficiency. Table 2 lists the most important configuration differences between the primary tracking and LRT sequences.

LRT tracks are seeded from SCT SPs only and a maximum of one seed per middle SP is allowed. This configuration is motivated by the displaced topology of tracks originating from LLP decays that often do not result in at least three Pixel SPs. No limit on the number of seeds is applied for confirmed seeds (only introduced for the updated LRT) and all such seeds are kept. To reflect the extended phase space of LRT tracks, criteria on the estimated impact parameters d_0 and z_0 are significantly relaxed. In contrast, the minimum p_{T} threshold is increased to 1 GeV to reduce the large number of soft charged pion tracks created in material interactions. The seed ordering in the primary pass uses $|d_0|$ as the defining criteria to order the relevance of seeds for the track finding stage (the seed with the lowest $|d_0|$ is ranked highest). This criteria is still relevant for tracks from LLP decays as the most probable $|d_0|$ value of such seeds is still small, owing to the exponential distribution of LLP lifetime. In addition, the LRT seed ordering includes a $\Delta\eta = |\eta_{\mathrm{seed}} - \eta'|$ weight factor, where η' is the pseudorapidity of the vector connecting the beam spot position with the point of closest approach of the seed. Seeds from LLP decays tend toward small values of $\Delta\eta$, due to the correlated direction of the LLP and its decay products, in contrast to seeds corresponding to fake tracks. These optimisations significantly improve the execution time by reducing the number of combinatorial permutations to process during the seed and track finding stages, without significantly changing the number of signal tracks being reconstructed.

Table 2 Most important selection criteria that differ between the primary tracking (*inside-out* sequence only) and LRT setups. Common selection criteria that were changed from the legacy implementation are also shown

Selection criteria	Primary	LRT
max. $\lvert d_0\rvert$ [mm]	5	300
max. $\lvert z_0\rvert$ [mm]	200	500
min. p_{T} [GeV]	0.5	1
max. $\lvert\eta\rvert$	2.7	3.0
max. silicon holes	2	1
max. double holes	1	0
max. holes gap	2	1
road width [mm]	12	5
seeding	Pixels and SCT	SCT only
max. seeds per middle Pixel SP	1	–
max. seeds per middle SCT SP	5	1
Common selection criteria		
min. silicon hits	8	
min. unshared silicon hits	6	
max. track χ^2/n_{DoF}	9	
keep all confirmed seeds	true	

The same relaxed impact parameter selections are imposed in the track finding and ambiguity solving steps. Other track selection criteria are significantly stricter for LRT tracks to ensure that a sufficiently low fake track rate is achieved. Tracks are required to pass the same strict silicon hit and track χ^2/n_{DoF} requirements as primary tracks. In addition, the maximum number of silicon holes is reduced to one, no double hole[7] on a track is allowed, and the search roads (sets of silicon detector modules that can be expected to contain

[7] A double whole is defined as two consecutive missing hits on active modules where both were expected based on the particle trajectory. In this context, the holes gap refers to the largest gap of consecutive missing hits on active modules (used in Table 2).

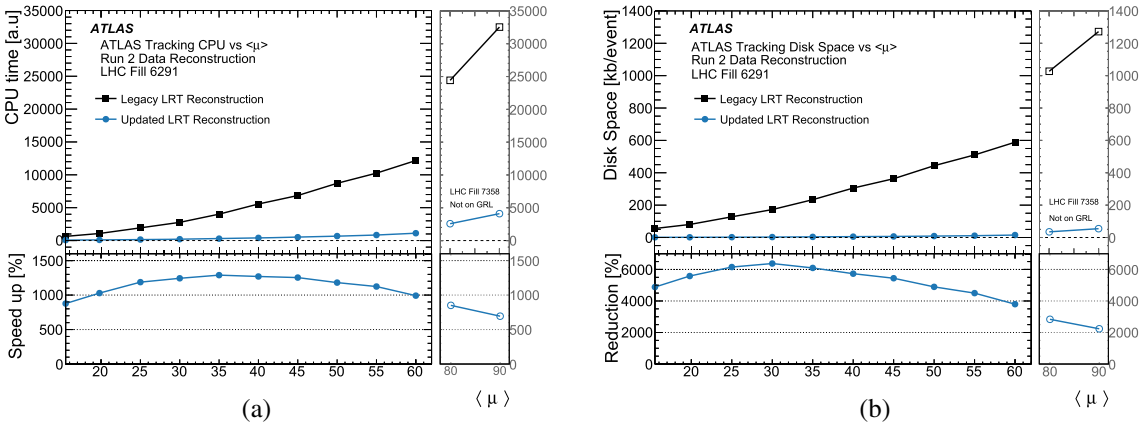

Fig. 5 The (**a**) processing time taken per event to reconstruct the same data events and (**b**) event size of the LRT reconstruction output, versus average pileup, comparing the legacy LRT and updated LRT reconstruction software. The high average pileup regime (open markers) with $\langle\mu\rangle > 80$ indicates data events taken from a 2018 machine development fill not passing the full ATLAS data quality requirements and therefore these are not included in the so-called 'Good Run List', GRL ('Not on GRL'). This range is included to provide an indication of the expected performance in such extreme pileup regimes

hits compatible with the seed) used to extend the seeds within the track finding stage are narrowed. These strict selections reduce the acceptance of tracks from LLP decays by less than 5% but they significantly reduce the number of low-quality tracks written to storage. Thus, they also lower the required number of iterations of the ambiguity resolution and TRT extension phases.

The resulting collection of tracks, whether they have a valid TRT extension or not, form the LRT track collection. The reduced total acceptance of LLP signal tracks compared to the legacy implementation is between 5 and 10% independent of the decay radius of the LLP. Detailed reconstruction efficiency studies of this new LRT pass are discussed in Sects. 5 and 6. When performing measurements or searches of new phenomena using the ATLAS data, the Poisson statistics of a counting experiment often results in a sensitivity related to $N_s/\sqrt{N_b}$, where N_s corresponds to the signal yield and N_b refers to the number of background events. A similar figure of merit, defined with the number of tracks originated from the LLP decays (N_{trk}^{LLP}) and from fake tracks (N_{trk}^{fake}), $N_{trk}^{LLP}/\sqrt{N_{trk}^{fake}}$ is used to quantify the impact of LRT on physics analyses. This figure of merit has improved by more than 400% for LHC Run 2 pileup conditions, making this third tracking pass a highly efficient reconstruction sequence. N_{trk}^{LLP} (N_{trk}^{fake}) is strongly correlated with N_s (N_b), however, this figure of merit here describes the LRT improvement and does not directly translate to equal sensitivity gains for LLP searches. Figure 5 shows the time to process[8] the LRT reconstruction and the output size of each event as a function of the average interactions per bunch crossing in 2018 data sample (no trigger or event topology selections applied). The processing time of the new implementation has improved by more than 10 times compared to the legacy implementation and the disk space usage per event for LRT tracks has been reduced by more than a factor of 50.

4.3 Truth-matching in simulation and fake tracks

In order to match a generated particle in simulation to a reconstructed track, a requirement (R_{match}) is applied that is defined by comparing the number of measurements in detector elements which are common between the truth particle trajectory and the reconstructed track:

$$R_{match} = \frac{10 \times N_{common}^{Pixel} + 5 \times N_{common}^{SCT} + N_{common}^{TRT}}{10 \times N_{reco}^{Pixel} + 5 \times N_{reco}^{SCT} + N_{reco}^{TRT}}, \quad (1)$$

where $N_{reco}^{Pixel/SCT/TRT}$ and $N_{common}^{Pixel/SCT/TRT}$ are the numbers of hits in the different detectors which are present on the reconstructed particle trajectory, and present on both the truth particle trajectory and the reconstructed track, respectively. The different weights applied to the different sub-detector are motivated by the different number of hits available in each sub-detector for the track reconstruction and the resolution of those hits. Sub-detectors with fewer hits are assigned with larger weights to ensure the truth matching does not favor one particular sub-detector. Reconstructed tracks with high values of R_{match} are considered well-matched to a truth particle and are used in efficiency calculations. Conversely, poorly-matched tracks (low values of R_{match}) are referred to as *fake tracks*. These tracks are dominated by incorrect combinations of hits from multiple particles in the pattern recognition. In

[8] All benchmark studies described in this work were run as the only active user on a dedicated machine equipped with an AMD EPYC™ 7302 16-core processor, running the CERN CENTOS 7 operating system. The processor was operated in 'performance' mode, with simultaneous multi-threading (SMT) and frequency boosting disabled.

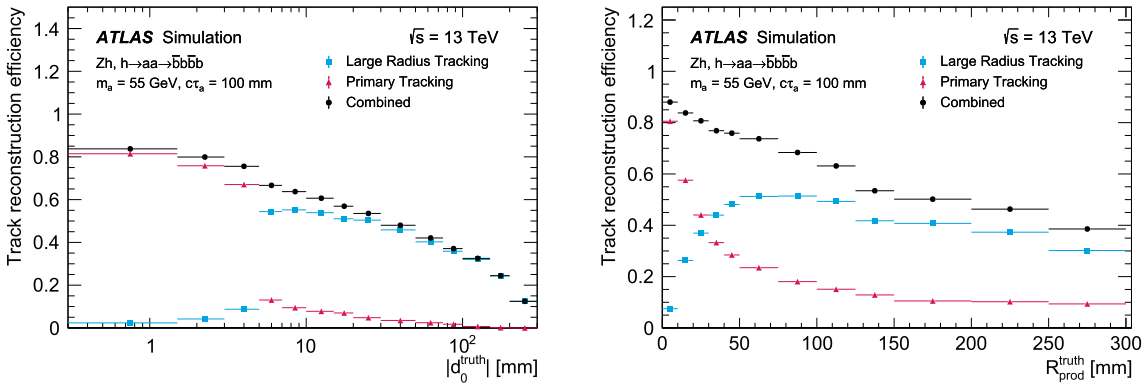

(a) (b)

Fig. 6 The primary, LRT, and combined track reconstruction efficiencies for displaced charged particles produced by the decay of the LLP in the Higgs portal signal model. Efficiencies are shown as a function of (**a**) $|d_0^{\text{truth}}|$ and (**b**) $R_{\text{prod}}^{\text{truth}}$. The first bin of **a** includes tracks with $|d_0^{\text{truth}}|$ down to $|d_0^{\text{truth}}| = 0$ mm. Truth particles are required to fulfill the fiducial selection criteria stated in the text

the following, $R_{\text{match}} > 0.5$ is used to identify well-matched tracks, while all other tracks are labelled fake tracks.

4.4 Secondary vertex reconstruction

Many analyses which used LRT in Run 2 attempted to reconstruct the decays of LLPs by performing an additional secondary vertex reconstruction using both primary and LRT tracks. To study how the improved LRT reconstruction performs in these downstream algorithms, two different secondary vertex reconstruction algorithms are used.

The first is a dedicated inclusive vertexing algorithm optimised for identifying the decays of heavy LLPs [58]. Vertices are formed from two-track seeds, which are required to contain at least one track with $|d_0| > 2$ mm. The compatibility of each possible pair of preselected tracks is then computed, and those deemed loosely-compatible are retained. These two-track seed vertices are then combined to form multi-track vertices using a pairwise compatibility graph. Nearby vertices are then merged, and lower-quality tracks not initially preselected for vertex seeding are attached to compatible vertices.

The second is an algorithm optimised for identifying two-body $V0$ decays (i.e. K^0 and Λ^0) [59]. Tracks are considered for vertex reconstruction if they are not associated to any primary pp interaction vertex (PV) [60], have $p_{\text{T}} > 1$ GeV, and satisfy $|d_0/\sigma_{d_0}| > 2$, where σ_{d_0} is the uncertainty on the reconstructed d_0. All opposite-charge two-track pairs are then considered. Vertices are kept if the χ^2/n_{DoF} probability of the two-track fit is greater than 0.0001. To reject vertices from random track combinations, selections are placed on the transverse ($a_{0,xy}$) and longitudinal ($a_{0,z}$) point of closest approach between the vertex flight direction[9] and the PV with the largest $\sum p_{\text{T}}^2$ of associated tracks. Vertices are kept if they satisfy $|a_{0,xy}| < 3$ mm and $|a_{0,z}| < 15$ mm. To reject residual contributions from combinations of prompt tracks, vertices are additionally required to have $L_{xy}/\sigma_{L_{xy}} > 2$, where L_{xy} is the transverse displacement of the vertex with respect to the primary vertex, and $\sigma_{L_{xy}}$ is its uncertainty.

5 Performance study on simulation

5.1 Reconstruction efficiency

To assess the track reconstruction efficiency in simulation, the hit-based matching scheme described in Sect. 4.3 is used to associate reconstructed tracks to generated particles. The track reconstruction efficiency is then defined as the ratio of the number of signal truth particles matched to reconstructed tracks divided by the number of signal truth particles. Truth particles are subject to fiducial selection described in Sect. 3. These requirements are chosen to be significantly far away from the selection criteria imposed in the LRT reconstruction in order to avoid turn-on effects due to reconstruction resolutions of track parameters.

The track reconstruction efficiencies for the Higgs portal benchmark models are shown in Fig. 6 as a function of $|d_0|$ and R_{prod}. The performance of the primary and LRT algorithms are compared together with the combination of the two. After $|d_0| > 5$ mm, the primary track reconstruction efficiency becomes significantly reduced, with LRT recovering the loss in efficiency with appreciable efficiencies out

[9] The vertex flight direction is defined as the direction of the vertex momentum vector, computed from the vectorial sum of the individual track momenta vectors.

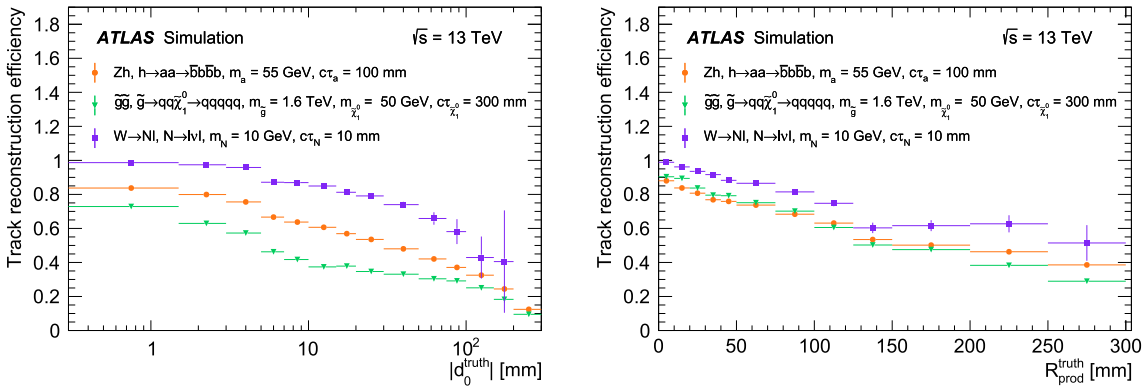

Fig. 7 Combined track reconstruction efficiency for displaced charged particles produced by the decay of long-lived signal particles in the long-lived neutralino, Higgs portal and heavy neutral lepton signal models. The efficiency is shown as a function of (**a**) $|d_0^{\text{truth}}|$ and (**b**) $R_{\text{prod}}^{\text{truth}}$. The first bin of **a** includes tracks with $|d_0^{\text{truth}}|$ down to $|d_0^{\text{truth}}| = 0$ mm. Truth particles are required to fulfill the fiducial selection criteria stated in the text

to $|d_0| = 300$ mm. This translates in a total efficiency of about 40% up to production radii of $R_{\text{prod}} = 300$ mm. A comparison of the combined track reconstruction efficiencies obtained for the three signal models considered is shown in Fig. 7. As expected, the combined efficiency degrades for dense environments in a given $|d_0|$ bin. In the region $10 < |d_0| < 20$ mm, the total track reconstruction efficiency is approximately 85%, 60% and 40% for heavy neutral lepton, the Higgs sector and long-lived neutralino benchmark models, respectively.

5.2 Robustness against pileup

As the average number of interactions per bunch crossing increases, so does the number of charged particles produced in an event. This increase in combinatorics can degrade the track reconstruction efficiency. The primary, LRT and combined track reconstruction efficiencies for the Higgs portal model are shown as a function of $\langle\mu\rangle$ in Fig. 8. The comparison of the combined efficiencies of the three benchmark signals is also provided showing more stable performance as a function of the pileup for tracks originated from leptonic decays. This effect is primarily due to the lack of hadronic interactions for leptonic signatures.

5.3 Impact on searches for displaced vertices

To evaluate the impact of the improved LRT configuration on searches for displaced vertices, it is useful to study how the updated track reconstruction changes the LLP vertex reconstruction efficiency. Additionally, it is important to investigate the overall rate of vertices reconstructed from fake tracks, which correspond to a dominant background in such searches. The study is performed using the Higgs portal benchmark model. To compare the performance between the two LRT configurations, the simulated events are reconstructed using the legacy and updated ATLAS track reconstruction configurations. Secondary vertices are reconstructed using the inclusive vertexing algorithm described in Sect. 4.4. Identical vertex reconstruction configurations are used for the two samples.

To assess the signal vertex reconstruction efficiency and evaluate the impact of fake tracks, a truth-matching procedure is performed. Reconstructed vertices are considered matched to an LLP decay if the p_{T}-weighted fraction of tracks in the vertex that are matched to truth-level LLP descendants (as described in Sect. 4.3) is greater than 0.5. Figure 9 shows the transverse displacement (L_{xy}) of truth-matched and non-truth-matched vertices for the legacy and improved reconstruction. The improved reconstruction has a modest increase in the number of LLP vertices and considerably fewer vertices not matched to LLP decays, non-LLP, due to the significant increase in purity of the LRT algorithm.

6 Data and simulation comparison

To further validate the improved LRT configuration, comparisons are performed between Run 2 data and simulated inelastic pp collisions. As mentioned in Sect. 3, the simulation is generated with a flat $\langle\mu\rangle$ profile and is thus reweighted to agree with the $\langle\mu\rangle$ profile of the data. The transverse momentum distributions of tracks are found to be consistent between data and simulation therefore no additional reweighting is performed. Track-level comparisons are performed (Sect. 6.1), as well as comparisons of the rate of fake reconstructed tracks (Sect. 6.2) and of the properties of sec-

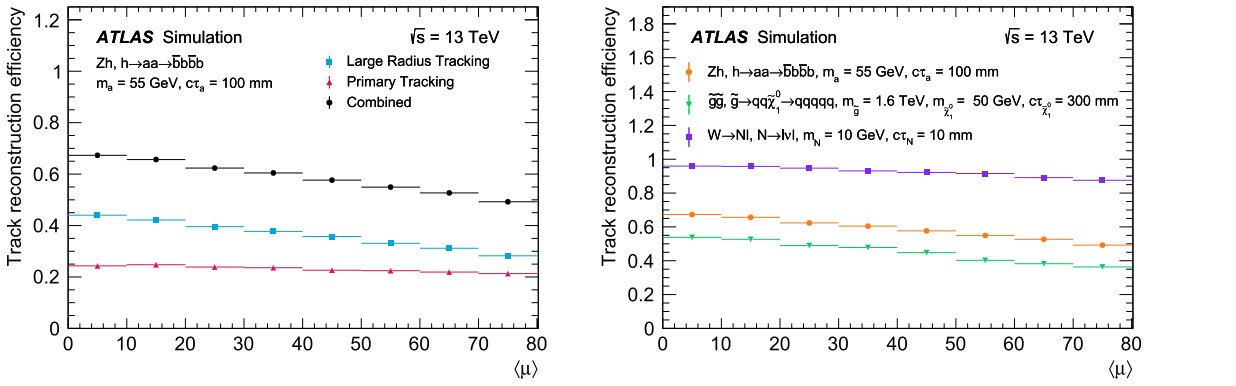

(a) (b)

Fig. 8 Track reconstruction efficiencies as a function of $\langle\mu\rangle$ for displaced charged particles produced by the decay of long-lived signal particles. (**a**) The primary, LRT and combined tracking efficiencies are compared for the Higgs portal model. (**b**) The combined efficiencies for the long-lived neutralino, Higgs portal and heavy neutral lepton signal models. Truth particles are required to fulfill the fiducial selection criteria stated in the text

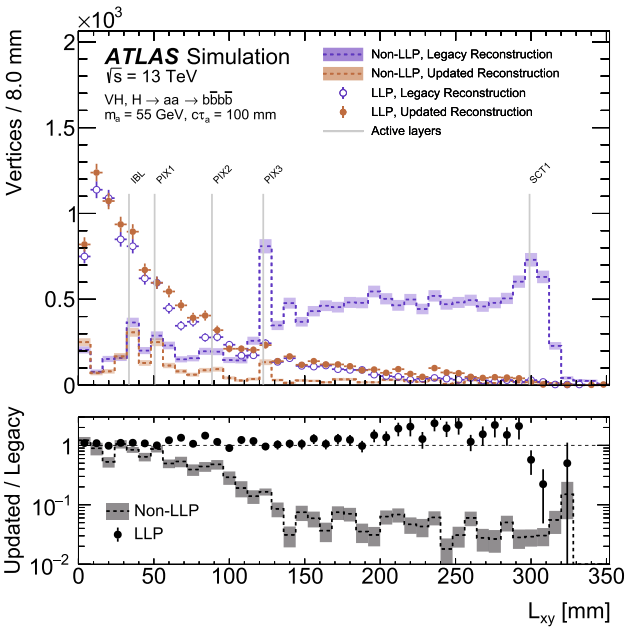

Fig. 9 A comparison of the radial distributions of reconstructed secondary vertices in a simulated LLP sample using the legacy and updated track reconstruction configurations. The circular markers represent reconstructed vertices that are matched to truth-level LLP decay vertices (LLP). The dashed lines represent reconstructed vertices that are not matched to truth-level LLP decay vertices (non-LLP). The radial position of the pixel and SCT detector layers are indicated by vertical lines. The lower panel shows the ratio of the number of vertices reconstructed in the updated reconstruction to those reconstructed in the legacy implementation for true LLP vertices (circular markers) and non-LLP vertices (dashed lines). The uncertainties shown are statistical only

ondary vertices consistent with the decays of K^0_S mesons (Sect. 6.3).

6.1 Track properties

The distributions of the number of hits in the pixel and SCT ID subsystems per LRT track are shown in Fig. 10, along with the distributions of $|d_0|$ and the radius of the first hit associated to the track. The largest deviations from unity in the ratio of data to simulation are at the 10% level. This is consistent with the performance of the Run 2 LRT configuration [13] and indicates good agreement between data and simulation. The peaks in the distribution of $|d_0|$ at 50 mm, 88 mm, and 122 mm coincide with the radial positions of the three pixel barrel layers, and correspond to low-p_{T} secondary tracks with trajectories tangential to the detector modules.

6.2 Fake rate

The number of tracks corresponding to real charged particle trajectories is expected to scale linearly with $\langle\mu\rangle$, since it is related to the number of charged particles produced in the collisions. However, during reconstruction, it is possible for the algorithm to reconstruct fake tracks not corresponding to real charged particle trajectories. The number of these random combinations is expected to scale with a higher power as a function of $\langle\mu\rangle$, since the increased combinatorics allow for more track candidates to be formed. The average number of primary tracks per event ($\langle N_{\mathrm{track,Prim.}}\rangle$) and the average number of LRT tracks per event ($\langle N_{\mathrm{track,LRT}}\rangle$) as a function of $\langle\mu\rangle$ is shown in Fig. 11 for data and simulation. To account for differences between the data and simulation in terms of the overall number of charged particles per event, an overall normalisation factor is used to adjust the number of tracks in simulation to data. This scale factor is determined to be 0.94, and is applied to simulation in both distributions.

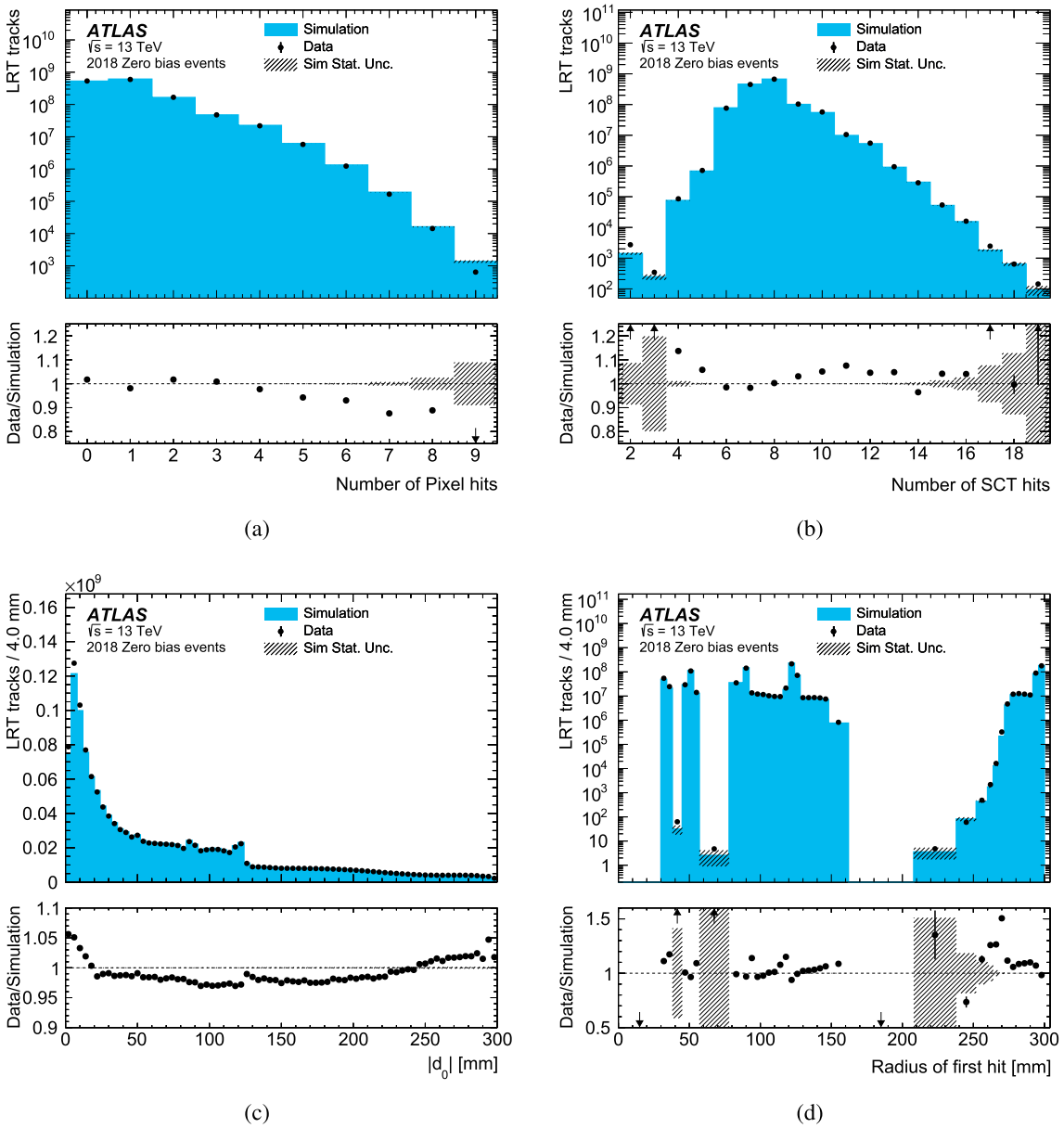

Fig. 10 The distribution of the number of hits in the (**a**) pixel and (**b**) SCT detector, (**c**) $|d_0|$, and (**d**) the radius of the first hit on each track, in 2018 zero bias data and simulated inelastic pp collisions. The simulation is normalised to the number of tracks in data. The statistical uncertainty on the data and simulation are shown as vertical error bars and shaded bands, respectively. Points in the ratio that do not lie within the visible range are shown as arrows

Comparing the distributions of $\langle N_{\text{track,Prim.}} \rangle$ to $\langle N_{\text{track,LRT}} \rangle$, it is clear that the fraction of fake tracks (deviation from linearity with $\langle \mu \rangle$) for the LRT reconstruction is significantly larger than for primary tracking. However, the overall number of tracks reconstructed by the LRT reconstruction is small compared to the number of primary tracks, indicating that the impact of the LRT fake rate is minimal to the overall size of the final track collection. Additionally, the difference between the measured value of $\langle N_{\text{track,LRT}} \rangle$ in simulation and data grows with increasing $\langle \mu \rangle$, indicating that the rate of fake tracks is larger in simulation than in data. This difference is driven by the modeling of the detector material in the simulation and will be discussed further in Sect. 6.3.1.

6.3 Study of K^0_S vertices

To compare the track reconstruction efficiency between data and simulation, a "standard candle" is needed to identify LRT tracks originating from a true LLP decay. The K^0_S meson is an ideal candidate due to its proper decay length ($c\tau = 27$ mm)

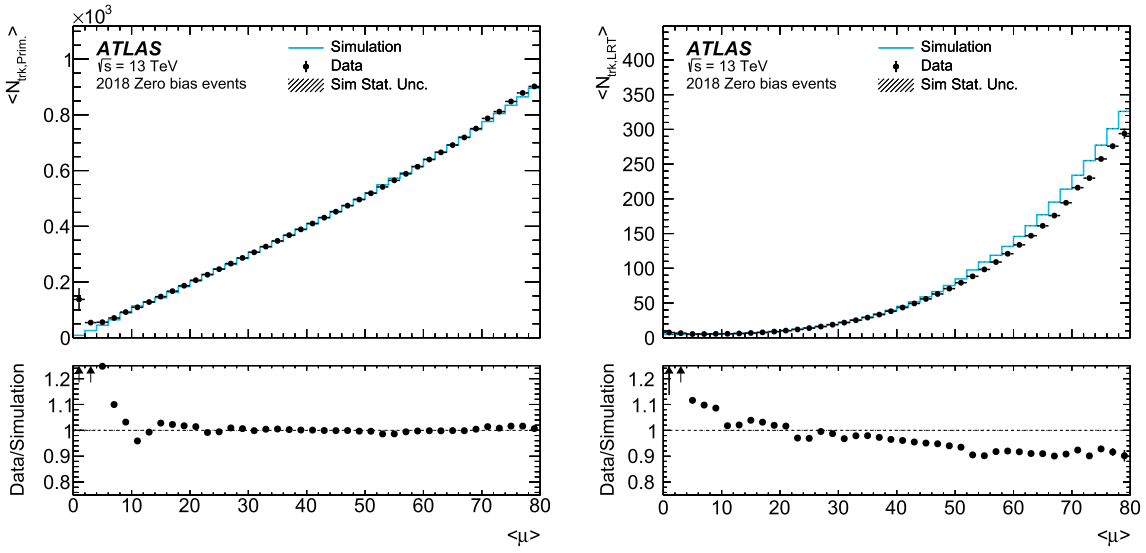

Fig. 11 The mean number of tracks per event as a function of $\langle\mu\rangle$ for (**a**) primary tracks and (**b**) LRT tracks. The simulation is scaled by extracting a scale factor from the ratio of $\langle N_{\text{track,Prim.}}\rangle$ of data to simulation

and a clean signature of a two-track vertex. To identify K_S^0 vertices, secondary vertices are reconstructed from the combined collection of primary and LRT tracks using the algorithm designed for reconstructing $V0$ decays described in Sect. 4.4. K_S^0 candidates are identified by requiring that the combined invariant mass of the two selected tracks is in the range [472, 522] MeV. No vetoes or background subtraction is applied to the vertices beyond those applied during reconstruction, as described in Sect. 4.4. The p_{T} distributions of the K_S^0 candidates were found to be well modeled in the simulation and thus no p_{T} re-weighting is applied. The distributions of the invariant mass of the K_S^0 candidates are shown for data and simulation in Fig. 12 for vertices with two primary tracks and two large radius tracks. The yields in simulation are normalised such that the number of K_S^0 candidates with two primary tracks agrees with the data. To assess the purity of the K_S^0 selection, the signal peak is fitted to a double-gaussian, and a third-order polynomial is used to extract the combinatorial background. Both distributions show very small combinatorial backgrounds with purities of roughly 99%.

The radial distribution (L_{xy}) of the reconstructed K_S^0 candidates are then compared between data and simulation, as shown in Fig. 13a. Vertices in simulation are separated in three categories, based on the number of LRT tracks included in the vertex fit. After the first SCT layer, LRT begins to have a diminishing contribution to the total yield. This is due to the fact that particles produced in this region will traverse an insufficient number of silicon layers to satisfy the hit requirements of inside-out track reconstruction and the primary outside-in tracking becomes dominant. Figure 13b shows the fraction of K_S^0 candidate vertices reconstructed with either two primary tracks or with at least one LRT track in data and simulation. The distributions are consistent between the two samples, further indicating good modeling of the LRT reconstruction in simulation. After $L_{xy} > 70$ mm, LRT tracks account for more than 75% of the total number of K_S^0 candidate vertices, highlighting the importance of LRT for the reconstruction of displaced vertices.

6.3.1 *Systematic uncertainty on the LRT reconstruction efficiency*

In Fig. 12b, a small difference can be observed between the number of K_S^0 candidates reconstructed with two LRT tracks between data and simulation, despite normalising the simulation such that a consistent number of candidates are reconstructed with two primary tracks. This indicates that there is a systematic difference between the LRT reconstruction efficiency measured in data and simulation. To account for this in physics analyses, a per-track uncertainty on the LRT reconstruction efficiency is derived by comparing the yields of LRT tracks associated to K_S^0 candidates as a function of $|\eta|$ and the radius of the first measurement on the track ($R_{1^{\text{st}}\text{ hit}}$). A summary of the measured relative uncertainties is provided in Table 3. To propagate these uncertainties to downstream object reconstruction algorithms such as secondary vertex reconstruction, a procedure is used in which tracks are randomly removed from the track collection considered by the vertex reconstruction with a probability corresponding to the per-track uncertainty of each track. This results in a modified vertex collection which can be used to assess the impact of

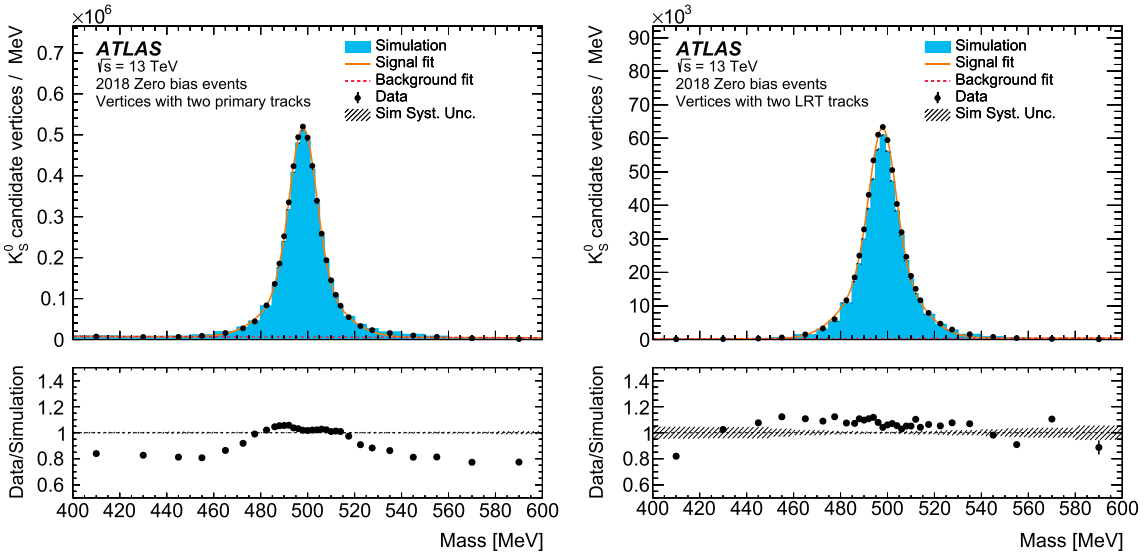

(a) (b)

Fig. 12 The invariant mass of K^0_S candidates reconstructed from (**a**) two primary tracks and (**b**) two LRT tracks, in 2018 zero bias data and simulated inelastic pp collisions. The signal peak is fitted to a double-gaussian, and a third-order polynomial is used to model the combinatorial background. The yields in simulation are normalised such that the number of K^0_S candidates with two primary tracks agrees with the data

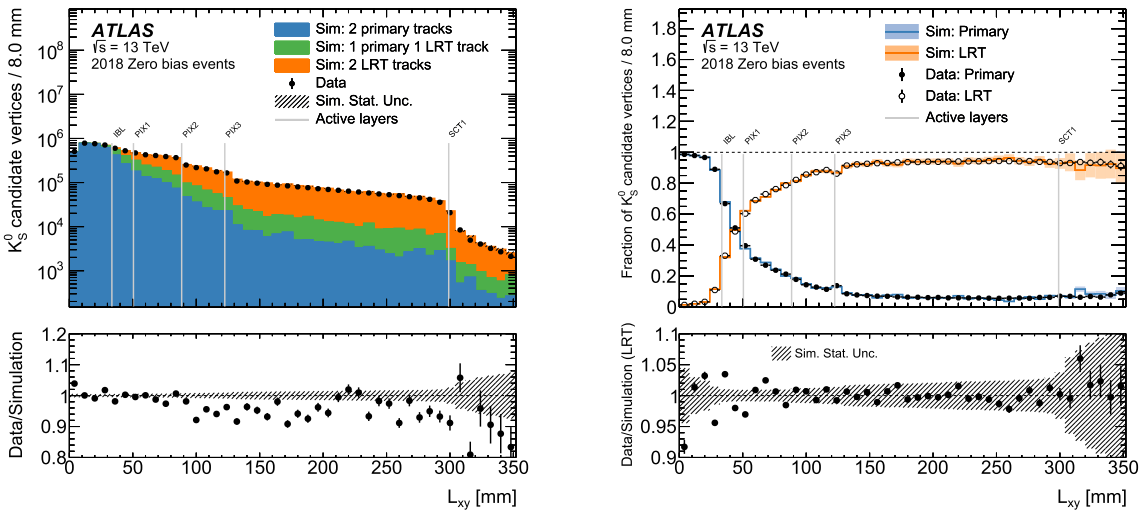

(a) (b)

Fig. 13 (**a**) The radial distribution of reconstructed K^0_S candidate vertices in 2018 zero bias data and simulated inelastic pp collisions. The yields in simulation are normalised such that the number of K^0_S candidates with two primary tracks agrees with the data. The lower panel displays the ratio between the total number of reconstructed K^0_S candidate vertices in the data and the simulation. The statistical uncertainty on the simulation is shown as a hatched band. (**b**) The fraction of K^0_S candidate vertices reconstructed with two primary tracks (labelled "Primary" in the legend) and at least one large radius track (labelled "LRT" in the legend) in 2018 zero bias data and simulated inelastic pp collisions. The four pixel layers and first SCT layer are shown in the figure with gray vertical lines. The lower panel displays the ratio between the fraction of reconstructed K^0_S candidate vertices with at least one LRT track in the data and the simulation

the per-track uncertainties on the final vertex reconstruction performance.

The average number of K^0_S candidate vertices per event is shown in Fig. 14 as a function of $\langle\mu\rangle$ for vertices with two primary tracks and two LRT tracks. In both cases, the simulation is scaled such that the total number of reconstructed K^0_S candidates with two primary tracks agrees with the data. Similar to the distributions of $\langle N_{\text{trk}}\rangle$, this is expected to scale

Table 3 The relative per-track uncertainties on the LRT reconstruction efficiency in various bins of $|\eta|$ and radius of the first measurement on the track $R_{1^{st}\,hit}$

$R_{1^{st}\,hit}$ [mm]	$\lvert\eta\rvert < 0.4$ (%)	$0.4 < \lvert\eta\rvert < 1.2$ (%)	$1.2 < \lvert\eta\rvert < 3.0$ (%)
[33.0, 38.0]	16.8	11.3	7.2
[46.0, 56.0]	10.0	4.3	5.6
[84.0, 94.0]	0.3	1.6	2.8
[118.0, 128.0]	0.8	3.9	6.6
[288.0, 320.0]	9.6	0.4	1.1

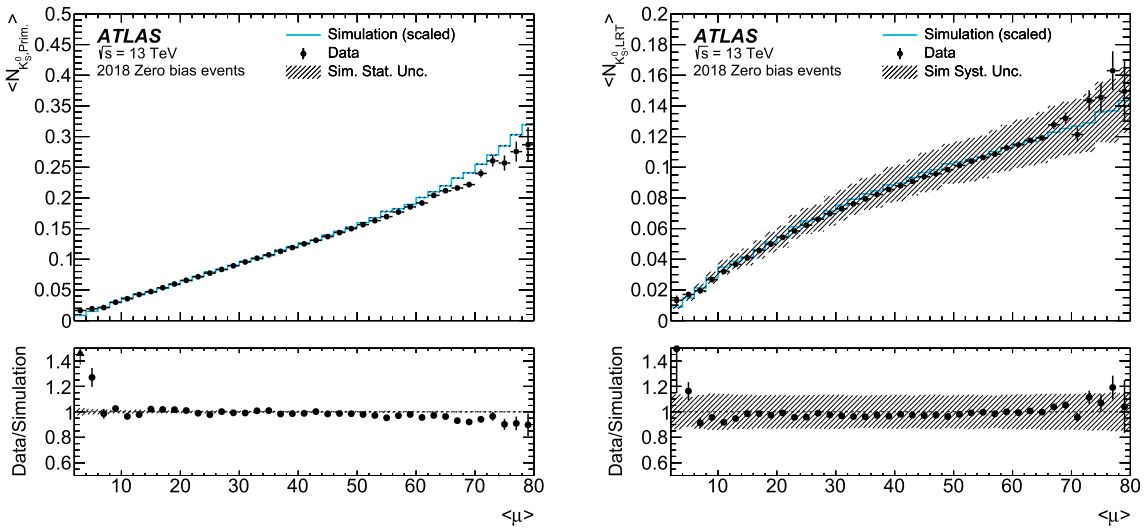

Fig. 14 The average number of K^0_S candidate vertices per event in 2018 zero bias data and simulated inelastic pp collisions shown as a function of the average number of interactions per bunch crossing $\langle\mu\rangle$ for (**a**) vertices with two primary tracks and (**b**) vertices with two LRT tracks. The simulation is scaled such that the total number of reconstructed K^0_S candidates with two primary tracks agrees with the data. The uncertainty on the simulation in (b) is derived by propagating the per-track uncertainties through to the vertex reconstruction using the method described in the text

linearly if the track reconstruction efficiency and proportion of background vertices stays constant as a function of $\langle\mu\rangle$. However, as $\langle\mu\rangle$ increases, so does the overall number of tracks in the event. This increases the probability for random track crossings that can mimic a K^0_S candidate, contributing to the deviation from linearity seen in Fig. 14a. For vertices with two LRT tracks however, Fig. 14b shows that the number of K^0_S candidate vertices starts to deviate downward from linearity. This indicates that even though the number of LRT fake tracks is high, the rate of fake vertices is relatively low. The main factor affecting the number of K^0_S candidates at high $\langle\mu\rangle$ values is the reduction in overall LRT reconstruction efficiency, as depicted in Fig. 8. The difference between the number of K^0_S candidate vertices per event in data and simulation shown in Fig. 14b is within the systematic uncertainties on the final vertex yields derived by propagating the per-track LRT uncertainties to the vertex reconstruction, as described above.

The discrepancy in yields can be attributed to the modeling of the Inner Detector material [21], and is explored further through an analysis of the alternate simulated samples described in Sect. 3. Three samples with modified detector geometries are considered: an overall 5% increase of the passive material in the ID, a 10% increase of the material in the IBL, and a 25% increase of the material describing the pixel services. A fourth sample is considered which uses the QGSP_BIC physics list instead of the nominal FTFP_BERT physics list in the GEANT4 simulation. Each simulated sample is first normalized such that the number of simulated events is consistent with the data. An additional normalisation factor is then applied to each sample, which is defined such that after normalisation the number of K^0_S candidates with two primary tracks in the nominal sample agrees with the data. The differences in yields between the nominal sample and the varied samples are then computed and used to derive an uncertainty band corresponding to each variation. The

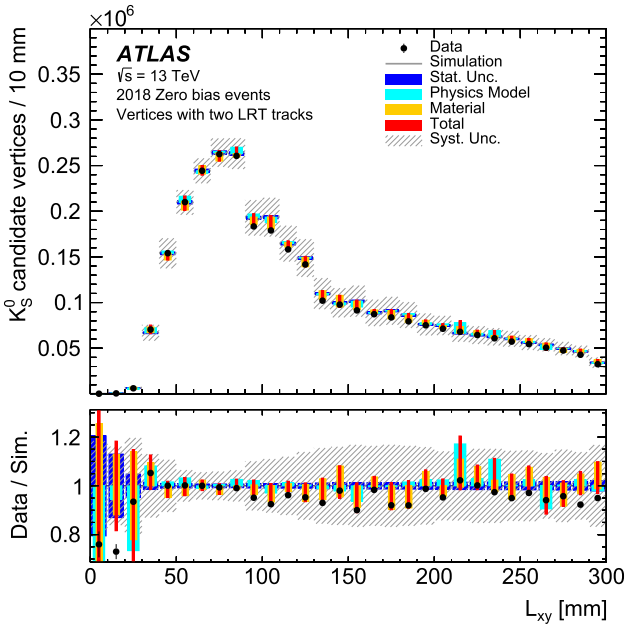

Fig. 15 The radial distribution of reconstructed K_S^0 candidate vertices with two LRT tracks in 2018 zero bias data and simulated inelastic pp collisions. The yields in simulation are normalised such that the number of K_S^0 candidates with two primary tracks agrees with the data. Samples with varied detector geometries and simulation parameters are used to derive uncertainties on the nominal simulation and are shown as filled bands. The uncertainties derived from each geometry variation are summed in quadrature to obtain a single uncertainty which is shown as an orange band (labeled "Material" in the legend). The uncertainty derived from comparing the nominal simulation to the sample with the modified physics list is shown as a light blue band (labeled "Physics Model" in the legend). The statistical uncertainty on the nominal sample is shown as a dark blue band (labeled "Stat. Unc." in the legend). The three sources of uncertainty (material, physics model, and statistical uncertainty) are then summed in quadrature to obtain a total uncertainty on each bin which is drawn as a red band (labeled "Total" in the legend). The systematic uncertainty derived following the method described in the text is shown as a hatched band (labeled "Syst. Unc." in the legend). The lower panel displays the ratio between the data and the nominal simulation and the relative values of each uncertainty

results of this analysis are shown in Fig. 15. The data yields are observed to fall within the range of values obtained from the set of varied simulated samples, indicating that the difference in LRT tracking efficiency between the data and the simulation is well characterised by these variations. Additionally, the systematic uncertainty derived by propagating the per-track LRT uncertainties to the vertex reconstruction is shown, and is found to cover the observed differences between the data and the simulation as well as the variations between the alternate simulated samples.

7 Conclusion

The ATLAS LRT algorithm has undergone significant improvements in preparation for Run 3 data taking. As a result of this reoptimisation, the processing time has improved by more than a factor of 10 and the disk space usage per event for LRT tracks has been reduced by more than a factor of 50 as compared to the legacy implementation, while still maintaining comparable track reconstruction efficiency. These improvements have allowed for LRT to be integrated in the standard ATLAS reconstruction chain. This will significantly simplify the workflow for future LLP analyses as well as allow for analyses not specifically targeting LLP signatures to benefit from increased track reconstruction efficiency at large $|d_0|$. A study of secondary vertex reconstruction for hadronic LLP signatures indicates that the improved LRT configuration leads to a significant reduction in vertices reconstructed from fake tracks and an overall improvement in the vertex reconstruction efficiency. This will translate directly to an improved signal to background ratio for displaced vertex searches in Run 3. To benefit from the improved performance, Run 2 data events have been reconstructed using these updated configurations. Additionally, comparisons between data and simulation show good modelling of both low-level track quantities as well as high-level properties of reconstructed K_S^0 vertices using LRT tracks. These developments are expected to increase the sensitivity of LLP searches in Run 3 and allow for a considerable expansion of the ATLAS LLP search program.

Acknowledgements We thank CERN for the very successful operation of the LHC, as well as the support staff from our institutions without whom ATLAS could not be operated efficiently.
We acknowledge the support of ANPCyT, Argentina; YerPhI, Armenia; ARC, Australia; BMWFW and FWF, Austria; ANAS, Azerbaijan; CNPq and FAPESP, Brazil; NSERC, NRC and CFI, Canada; CERN; ANID, Chile; CAS, MOST and NSFC, China; Minciencias, Colombia; MEYS CR, Czech Republic; DNRF and DNSRC, Denmark; IN2P3-CNRS and CEA-DRF/IRFU, France; SRNSFG, Georgia; BMBF, HGF and MPG, Germany; GSRI, Greece; RGC and Hong Kong SAR, China; ISF and Benoziyo Center, Israel; INFN, Italy; MEXT and JSPS, Japan; CNRST, Morocco; NWO, Netherlands; RCN, Norway; MEiN, Poland; FCT, Portugal; MNE/IFA, Romania; MESTD, Serbia; MSSR, Slovakia; ARRS and MIZŠ, Slovenia; DSI/NRF, South Africa; MICINN, Spain; SRC and Wallenberg Foundation, Sweden; SERI, SNSF and Cantons of Bern and Geneva, Switzerland; MOST, Taiwan; TENMAK, Türkiye; STFC, United Kingdom; DOE and NSF, USA. In addition, individual groups and members have received support from BCKDF, CANARIE, Compute Canada and CRC, Canada; PRIMUS 21/SCI/017 and UNCE SCI/013, Czech Republic; COST, ERC, ERDF, Horizon 2020 and Marie Skłodowska-Curie Actions, European Union; Investissements d'Avenir Labex, Investissements d'Avenir Idex and ANR, France; DFG and AvH Foundation, Germany; Herakleitos, Thales and Aristeia programmes co-financed by EU-ESF and the Greek NSRF, Greece; BSF-NSF and MINERVA, Israel; Norwegian Financial Mechanism 2014-2021, Norway; NCN and NAWA, Poland; La Caixa Banking Foundation, CERCA Programme Generalitat de Catalunya and PROMETEO and GenT Pro-

grammes Generalitat Valenciana, Spain; Göran Gustafssons Stiftelse, Sweden; The Royal Society and Leverhulme Trust, United Kingdom.
The crucial computing support from all WLCG partners is acknowledged gratefully, in particular from CERN, the ATLAS Tier-1 facilities at TRIUMF (Canada), NDGF (Denmark, Norway, Sweden), CC-IN2P3 (France), KIT/GridKA (Germany), INFN-CNAF (Italy), NL-T1 (Netherlands), PIC (Spain), ASGC (Taiwan), RAL (UK) and BNL (USA), the Tier-2 facilities worldwide and large non-WLCG resource providers. Major contributors of computing resources are listed in Ref. [61].

Data Availability Statement This manuscript has no associated data or the data will not be deposited. [Authors' comment: All ATLAS scientific output is published in journals, and preliminary results are made available in Conference Notes. All are openly available, without restriction on use by external parties beyond copyright law and the standard conditions agreed by CERN. Data associated with journal publications are also made available: tables and data from plots (e.g. cross section values, likelihood profiles, selection efficiencies, cross section limits, ...) are stored in appropriate repositories such as HEPDATA (http://hepdata.cedar.ac.uk/). ATLAS also strives to make additional material related to the paper available that allows a reinterpretation of the data in the context of new theoretical models. For example, an extended encapsulation of the analysis is often provided for measurements in the framework of RIVET (http://rivet.hepforge.org/)." This information is taken from the ATLAS Data Access Policy, which is a public document that can be downloaded from http://opendata.cern.ch/record/413 [opendata.cern.ch].]

Funded by SCOAP[3]. SCOAP[3] supports the goals of the International Year of Basic Sciences for Sustainable Development.

References

1. LHC Machine, JINST 3 (2008) S08001, ed. by L. Evans and P. Bryant
2. M. Gronau, C.N. Leung, J.L. Rosner, Extending limits on neutral heavy leptons. Phys. Rev. D **29**(11), 2539 (1984). https://doi.org/10.1103/PhysRevD.29.2539
3. M.J. Strassler, K.M. Zurek, Discovering the Higgs through highly-displaced vertices. Phys. Lett. B **661**, 263 (2008). (**ISSN: 0370-2693**)
4. J. Alimena et al., Searching for long-lived particles beyond the Standard Model at the Large Hadron Collider. J. Phys. G Nucl. Part. Phys. **47**, 090501 (2020). https://doi.org/10.1088/1361-6471/ab4574
5. ATLAS Collaboration, Search for long-lived, massive particles in events with displaced vertices and missing transverse momentum in $\sqrt{s} = 13\,TeV$ pp collisions with the ATLAS detector. Phys. Rev. D **97**, 052012 (2018). arXiv:1710.04901 [hep-ex]
6. ATLAS Collaboration, Search for displaced vertices of oppositely charged leptons from decays of long-lived particles in pp collisions at $\sqrt{s} = 13\,TeV$ with the ATLAS detector. Phys. Lett. B **801**, 135114 (2020). arXiv:1907.10037 [hep-ex]
7. ATLAS Collaboration, Search for long-lived neutral particles produced in pp collisions at $\sqrt{s} = 13\,TeV$ decaying into displaced hadronic jets in the ATLAS inner detector and muon spectrometer. Phys. Rev. D **101**, 052013 (2020). arXiv:1911.12575 [hep-ex]
8. ATLAS Collaboration, Search for long-lived, massive particles in events with a displaced vertex and a muon with large impact parameter in pp collisions at $\sqrt{s} = 13\,TeV$ with the ATLAS detector. Phys. Rev. D **102**, 032006 (2020). arXiv:2003.11956 [hep-ex]
9. ATLAS Collaboration, Search for displaced leptons in $\sqrt{s} = 13\,TeV$ pp collisions with the ATLAS detector. Phys. Rev. Lett. **127**, 051802 (2020). arXiv: 2011.07812 [hep-ex]
10. ATLAS Collaboration, Search for exotic decays of the Higgs boson into long-lived particles in pp collisions at $\sqrt{s} = 13\,TeV$ using displaced vertices in the ATLAS inner detector. JHEP **11**, 229 (2021). arXiv: 2107.06092 [hep-ex]
11. ATLAS Collaboration, Search for heavy neutral leptons in decays of W bosons using a dilepton displaced vertex in $\sqrt{s} = 13\,TeV$ pp collisions with the ATLAS detector (2022). arXiv:2204.11988 [hep-ex]
12. ATLAS Collaboration, Search for long-lived, massive particles in events with displaced vertices and multiple jets in pp collisions at $\sqrt{s} = 13\,TeV$ with the ATLAS detector (2023). arXiv:2301.13866 [hep-ex]
13. ATLAS Collaboration, Performance of the reconstruction of large impact parameter tracks in the inner detector of ATLAS, ATL-PHYS-PUB-2017-014 (2017). https://cds.cern.ch/record/2275635
14. ATLAS Collaboration, Software Performance of the ATLAS Track Reconstruction for LHC Run 3, ATL-PHYS-PUB-2021-012 (2021). https://cds.cern.ch/record/2766886
15. ATLAS Collaboration, ATLAS data quality operations and performance for 2015–2018 data-taking. JINST 15 (2020) P04003. arXiv:1911.04632 [physics.ins-det]
16. ATLAS Collaboration, The ATLAS Experiment at the CERN Large Hadron Collider. JINST **3**, S08003 (2008)
17. ATLAS Collaboration, 2015 start-up trigger menu and initial performance assessment of the ATLAS trigger using Run-2 data, ATL-DAQ-PUB-2016-001 (2016). https://cds.cern.ch/record/2136007
18. ATLAS Collaboration, The ATLAS Collaboration Software and Firmware, ATL-SOFT-PUB-2021-001 (2021). https://cds.cern.ch/record/2767187
19. ATLAS Collaboration, ATLAS Inner Detector: Technical Design Report, Volume 1, ATLAS-TDR-4; CERN-LHCC-97-016 (1997). https://cds.cern.ch/record/331063
20. ATLAS Collaboration, ATLAS Inner Detector: Technical Design Report, Volume 2, ATLAS-TDR-5, CERN-LHCC-97-017 (1997). https://cds.cern.ch/record/331064
21. ATLAS Collaboration, Study of the material of the ATLAS inner detector for Run 2 of the LHC. JINST **12**, P12009 (2017). arXiv:1707.02826 [hep-ex]
22. ATLAS Collaboration, ATLAS Insertable B-Layer: Technical Design Report, ATLAS-TDR-19; CERN-LHCC-2010-013 (2010). https://cds.cern.ch/record/1291633, Addendum: ATLAS-TDR-19-ADD-1; CERN-LHCC-2012-009 (2012). https://cds.cern.ch/record/1451888
23. B. Abbott et al., Production and integration of the ATLAS Insertable B-Layer. JINST **13**, T05008 (2018). arXiv:1803.00844 [physics.ins-det]
24. ATLAS Collaboration, Operation and performance of the ATLAS semiconductor tracker. JINST **9**, P08009 (2014). arXiv:1404.7473 [hep-ex]

25. ATLAS Collaboration, Performance of the ATLAS Transition Radiation Tracker in Run 1 of the LHC: tracker properties. JINST **12**, P05002 (2017). arXiv:1702.06473 [hep-ex]
26. G.R. Farrar, P. Fayet, Phenomenology of the production, decay, and detection of new hadronic states associated with supersymmetry. Phys. Lett. B **76**, 575 (1978)
27. L.J. Hall, M. Suzuki, Explicit R-parity breaking in supersymmetric models. Nucl. Phys. B **231**, 419 (1984)
28. G.G. Ross, J.W.F. Valle, Supersymmetric models without R-parity. Phys. Lett. B **151**, 375 (1985)
29. V.D. Barger, G.F. Giudice, T. Han, Some new aspects of supersymmetry R-parity violating interactions. Phys. Rev. D **40**, 2987 (1989)
30. H.K. Dreiner, An Introduction to explicit R-parity violation. Adv. Ser. Direct. High Energy Phys. **21**, 565 (2010). arXiv:hep-ph/9707435
31. R. Barbier et al., R-parity violating supersymmetry. Phys. Rep. **420**, 1 (2005). arXiv:hep-ph/0406039
32. B.C. Allanach, A. Dedes, H.K. Dreiner, R parity violating minimal supergravity model. Phys. Rev. D **69**, 115002 (2004) (**Erratum: Phys.Rev.D 72, 079902 (2005)**). arXiv:hep-ph/0309196
33. J. Alwall et al., The automated computation of tree-level and next-to-leading order differential cross sections, and their matching to parton shower simulations. JHEP **07**, 079 (2014). arXiv:1405.0301 [hep-ph]
34. T. Sjostrand et al., An introduction to PYTHIA 8.2. Comput. Phys. Commun. **191**, 159 (2015). arXiv:1410.3012 [hep-ph]
35. ATLAS Collaboration, ATLAS Pythia 8 tunes to 7 TeV data, ATL-PHYS-PUB-2014-021 (2014). https://cds.cern.ch/record/1966419
36. NNPDF Collaboration, Parton distributions for the LHC Run II, JHEP 04 (2015) 040. arXiv:1410.8849 [hep-ph]
37. R.M. Schabinger, J.D. Wells, A minimal spontaneously broken hidden sector and its impact on Higgs boson physics at the large hadron collider. Phys. Rev. D **72**, 093007 (2005). arXiv:hep-ph/0509209
38. B. Patt, F. Wilczek, Higgs-field portal into hidden sectors (2006). MIT-CTP-3745, arXiv:hep-ph/0605188
39. M.J. Strassler, K.M. Zurek, Echoes of a hidden valley at hadron colliders. Phys. Lett. B **651**, 374 (2007). arXiv:hep-ph/0604261
40. M.J. Strassler, K.M. Zurek, Discovering the Higgs through highly-displaced vertices. Phys. Lett. B **661**, 263 (2008). arXiv:hep-ph/0605193
41. S. Alioli, P. Nason, C. Oleari, E. Re, A general framework for implementing NLO calculations in shower Monte Carlo programs: the POWHEG BOX. JHEP **06**, 043 (2010). arXiv:1002.2581 [hep-ph]
42. G. Cullen et al., Automated one-loop calculations with GoSam. Eur. Phys. J. C **72**, 1889 (2012). arXiv:1111.2034 [hep-ph]
43. J. Butterworth et al., PDF4LHC recommendations for LHC Run II. J. Phys. G **43**, 023001 (2016). arXiv:1510.03865 [hep-ph]
44. ATLAS Collaboration, Measurement of the Z/γ^* boson transverse momentum distribution in pp collisions at $\sqrt{s} = 7TeV$ with the ATLAS detector. JHEP **09**, 145, arXiv:1406.3660 [hep-ex]
45. T. Asaka, M. Shaposhnikov, The νMSM, dark matter and baryon asymmetry of the universe. Phys. Lett. B **620**, 17 (2005). arXiv:hep-ph/0505013
46. L. Canetti, M. Drewes, M. Shaposhnikov, Sterile neutrinos as the origin of dark and baryonic matter. Phys. Rev. Lett. **110**, 061801 (2013). arXiv:1204.3902 [hep-ph]
47. M. Gronau, C.N. Leung, J.L. Rosner, Extending limits on neutral heavy leptons. Phys. Rev. D **29**(11), 2539 (1984). https://doi.org/10.1103/PhysRevD.29.2539
48. K. Bondarenko, A. Boyarsky, D. Gorbunov, O. Ruchayskiy, Phenomenology of GeV-scale heavy neutral leptons. JHEP **11**, 032 (2018). arXiv:1805.08567 [hep-ph]
49. ATLAS Collaboration, Operation of the ATLAS trigger system in Run 2. JINST **15**, P10004 (2020). arXiv:2007.12539 [hep-ex]
50. T. Pierog, I. Karpenko, J.M. Katzy, E. Yatsenko, K. Werner, EPOS LHC: test of collective hadronization with data measured at the CERN Large Hadron Collider. Phys. Rev. C **92**, 034906 (2015). arXiv:1306.0121 [hep-ph]
51. ATLAS Collaboration, The Pythia 8 A3 tune description of ATLAS minimum bias and inelastic measurements incorporating the Donnachie. Landshoff diffractive model, ATL-PHYS-PUB-2016-017 (2016). https://cds.cern.ch/record/2206965
52. J. Allison et al., Recent developments in Geant4. Nucl. Instrum. Methods Phys. Res. Sect. A Accel. Spectrom. Detect. Assoc. Equip. **835**, 186 (2016) (**ISSN: 0168-9002**)
53. ATLAS Collaboration, Characterization of Interaction-Point Beam Parameters Using the pp Event-Vertex Distribution Reconstructed in the ATLAS Detector at the LHC, ATLAS-CONF-2010-027 (2010). https://cds.cern.ch/record/1277659
54. R. Mankel, A concurrent track evolution algorithm for pattern recognition in the HERA-B main tracking system. Nucl. Instrum. Methods Phys. Res. Sect. A Accel. Spectrom. Detect. Assoc. Equip. **395**, 169 (1997) (**ISSN: 0168-9002**)
55. R. Fruhwirth, Application of Kalman filtering to track and vertex fitting. Nucl. Instrum. Methods Phys. Res. Sect. A Accel. Spectrom. Detect. Assoc. Equip. **262**, 444 (1987) (**ISSN:0168-9002**)
56. ATLAS Collaboration, Performance of the ATLAS track reconstruction algorithms in dense environments in LHC Run 2. Eur. Phys. J. C **77**, 673 (2017). arXiv:1704.07983 [hep-ex]
57. ATLAS Collaboration, Alignment of the ATLAS Inner Detector in Run-2. Eur. Phys. J. C **80**, 1194 (2020). arXiv:2007.07624 [hep-ex]
58. ATLAS Collaboration, Performance of vertex reconstruction algorithms for detection of new long-lived particle decays within the ATLAS inner detector, ATL-PHYS-PUB-2019-013 (2019). https://cds.cern.ch/record/2669425
59. ATLAS Collaboration, K^0_S and Λ production in pp interactions at $\sqrt{s} = 0.9 and 7 TeV$ measured with the ATLAS detector at the LHC. Phys. Rev. D **85**, 012001 (2012). arXiv: 1111.1297 [hep-ex]
60. ATLAS Collaboration, Development of ATLAS Primary Vertex Reconstruction for LHC Run 3, ATL-PHYS-PUB-2019-015 (2019). https://cds.cern.ch/record/2670380
61. ATLAS Collaboration, ATLAS Computing Acknowledgements, ATL-SOFT-PUB-2021-003 (2021). https://cds.cern.ch/record/2776662

ATLAS Collaboration[*]

G. Aad[102], B. Abbott[120], K. Abeling[55], N. J. Abicht[49], S. H. Abidi[29], A. Aboulhorma[35e], H. Abramowicz[151], H. Abreu[150], Y. Abulaiti[117], A. C. Abusleme Hoffman[137a], B. S. Acharya[69a,69b,q], C. Adam Bourdarios[4], L. Adamczyk[86a], L. Adamek[155], S. V. Addepalli[26], M. J. Addison[101], J. Adelman[115], A. Adiguzel[21c], T. Adye[134], A. A. Affolder[136], Y. Afik[36], M. N. Agaras[13], J. Agarwala[73a,73b], A. Aggarwal[100], C. Agheorghiesei[27c], A. Ahmad[36], F. Ahmadov[38,ae], W. S. Ahmed[104], S. Ahuja[95], X. Ai[62a], G. Aielli[76a,76b], M. Ait Tamlihat[35e], B. Aitbenchikh[35a], I. Aizenberg[169], M. Akbiyik[100], T. P. A. Åkesson[98], A. V. Akimov[37], D. Akiyama[168], N. N. Akolkar[24], K. Al Khoury[41], G. L. Alberghi[23b], J. Albert[165], P. Albicocco[53], G. L. Albouy[60], S. Alderweireldt[52], M. Aleksa[36], I. N. Aleksandrov[38], C. Alexa[27b], T. Alexopoulos[10], A. Alfonsi[114], F. Alfonsi[23b], M. Algren[56], M. Alhroob[120], B. Ali[132], H. M. J. Ali[91], S. Ali[148], S. W. Alibocus[92], M. Aliev[37], G. Alimonti[71a], W. Alkakhi[55], C. Allaire[66], B. M. M. Allbrooke[146], J. F. Allen[52], C. A. Allendes Flores[137f], P. P. Allport[20], A. Aloisio[72a,72b], F. Alonso[90], C. Alpigiani[138], M. Alvarez Estevez[99], A. Alvarez Fernandez[100], M. Alves Cardoso[56], M. G. Alviggi[72a,72b], M. Aly[101], Y. Amaral Coutinho[83b], A. Ambler[104], C. Amelung[36], M. Amerl[101], C. G. Ames[109], D. Amidei[106], S. P. Amor Dos Santos[130a], K. R. Amos[163], V. Ananiev[125], C. Anastopoulos[139], T. Andeen[11], J. K. Anders[36], S. Y. Andrean[47a,47b], A. Andreazza[71a,71b], S. Angelidakis[9], A. Angerami[41,ai], A. V. Anisenkov[37], A. Annovi[74a], C. Antel[56], M. T. Anthony[139], E. Antipov[145], M. Antonelli[53], D. J. A. Antrim[17a], F. Anulli[75a], M. Aoki[84], T. Aoki[153], J. A. Aparisi Pozo[163], M. A. Aparo[146], L. Aperio Bella[48], C. Appelt[18], A. Apyan[26], N. Aranzabal[36], C. Arcangeletti[53], A. T. H. Arce[51], E. Arena[92], J.-F. Arguin[108], S. Argyropoulos[54], J.-H. Arling[48], O. Arnaez[4], H. Arnold[114], Z. P. Arrubarrena Tame[109], G. Artoni[75a,75b], H. Asada[111], K. Asai[118], S. Asai[153], N. A. Asbah[61], J. Assahsah[35d], K. Assamagan[29], R. Astalos[28a], S. Atashi[160], R. J. Atkin[33a], M. Atkinson[162], N. B. Atlay[18], H. Atmani[62b], P. A. Atmasiddha[106], K. Augsten[132], S. Auricchio[72a,72b], A. D. Auriol[20], V. A. Austrup[101], G. Avolio[36], K. Axiotis[56], G. Azuelos[108,an], D. Babal[28b], H. Bachacou[135], K. Bachas[152,u], A. Bachiu[34], F. Backman[47a,47b], A. Badea[61], P. Bagnaia[75a,75b], M. Bahmani[18], A. J. Bailey[163], V. R. Bailey[162], J. T. Baines[134], L. Baines[94], C. Bakalis[10], O. K. Baker[172], E. Bakos[15], D. Bakshi Gupta[8], R. Balasubramanian[114], E. M. Baldin[37], P. Balek[86a], E. Ballabene[23a,23b], F. Balli[135], L. M. Baltes[63a], W. K. Balunas[32], J. Balz[100], E. Banas[87], M. Bandieramonte[129], A. Bandyopadhyay[24], S. Bansal[24], L. Barak[151], M. Barakat[48], E. L. Barberio[105], D. Barberis[57a,57b], M. Barbero[102], G. Barbour[96], K. N. Barends[33a], T. Barillari[110], M.-S. Barisits[36], T. Barklow[143], P. Baron[122], D. A. Baron Moreno[101], A. Baroncelli[62a], G. Barone[29], A. J. Barr[126], J. D. Barr[96], L. Barranco Navarro[47a,47b], F. Barreiro[99], J. Barreiro Guimarães da Costa[14a], U. Barron[151], M. G. Barros Teixeira[130a], S. Barsov[37], F. Bartels[63a], R. Bartoldus[143], A. E. Barton[91], P. Bartos[28a], A. Basan[100], M. Baselga[49], A. Bassalat[66,b], M. J. Basso[156a], C. R. Basson[101], R. L. Bates[59], S. Batlamous[35e], J. R. Batley[32], B. Batool[141], M. Battaglia[136], D. Battulga[18], M. Bauce[75a,75b], M. Bauer[36], P. Bauer[24], L. T. Bazzano Hurrell[30], J. B. Beacham[51], T. Beau[127], P. H. Beauchemin[158], F. Becherer[54], P. Bechtle[24], H. P. Beck[19,t], K. Becker[167], A. J. Beddall[82], V. A. Bednyakov[38], C. P. Bee[145], L. J. Beemster[15], T. A. Beermann[36], M. Begalli[83d], M. Begel[29], A. Behera[145], J. K. Behr[48], J. F. Beirer[55], F. Beisiegel[24], M. Belfkir[159], G. Bella[151], L. Bellagamba[23b], A. Bellerive[34], P. Bellos[20], K. Beloborodov[37], N. L. Belyaev[37], D. Benchekroun[35a], F. Bendebba[35a], Y. Benhammou[151], M. Benoit[29], J. R. Bensinger[26], S. Bentvelsen[114], L. Beresford[48], M. Beretta[53], E. Bergeaas Kuutmann[161], N. Berger[4], B. Bergmann[132], J. Beringer[17a], G. Bernardi[5], C. Bernius[143], F. U. Bernlochner[24], F. Bernon[36,102], T. Berry[95], P. Berta[133], A. Berthold[50], I. A. Bertram[91], S. Bethke[110], A. Betti[75a,75b], A. J. Bevan[94], M. Bhamjee[33c], S. Bhatta[145], D. S. Bhattacharya[166], P. Bhattarai[26], V. S. Bhopatkar[121], R. Bi[29,ap], R. M. Bianchi[129], G. Bianco[23a,23b], O. Biebel[109], R. Bielski[123], M. Biglietti[77a], T. R. V. Billoud[132], M. Bindi[55], A. Bingul[21b], C. Bini[75a,75b], A. Biondini[92], C. J. Birch-sykes[101], G. A. Bird[20,134], M. Birman[169], M. Biros[133], T. Bisanz[49], E. Bisceglie[43a,43b], D. Biswas[141], A. Bitadze[101], K. Bjørke[125], I. Bloch[48], C. Blocker[26], A. Blue[59], U. Blumenschein[94], J. Blumenthal[100], G. J. Bobbink[114], V. S. Bobrovnikov[37], M. Boehler[54], B. Boehm[166], D. Bogavac[36], A. G. Bogdanchikov[37], C. Bohm[47a], V. Boisvert[95], P. Bokan[48], T. Bold[86a], M. Bomben[5], M. Bona[94], M. Boonekamp[135], C. D. Booth[95], A. G. Borbély[59], I. S. Bordulev[37], H. M. Borecka-Bielska[108], L. S. Borgna[96], G. Borissov[91], D. Bortoletto[126], D. Boscherini[23b], M. Bosman[13], J. D. Bossio Sola[36], K. Bouaouda[35a], N. Bouchhar[163], J. Boudreau[129], E. V. Bouhova-Thacker[91], D. Boumediene[40], R. Bouquet[5], A. Boveia[119], J. Boyd[36], D. Boye[29], I. R. Boyko[38], J. Bracinik[20], N. Brahimi[62d], G. Brandt[171], O. Brandt[32], F. Braren[48],

B. Brau[103], J. E. Brau[123], R. Brener[169], L. Brenner[114], R. Brenner[161], S. Bressler[169], D. Britton[59], D. Britzger[110], I. Brock[24], G. Brooijmans[41], W. K. Brooks[137f], E. Brost[29], L. M. Brown[165,n], L. E. Bruce[61], T. L. Bruckler[126], P. A. Bruckman de Renstrom[87], B. Brüers[48], D. Bruncko[28b,*], A. Bruni[23b], G. Bruni[23b], M. Bruschi[23b], N. Bruscino[75a,75b], T. Buanes[16], Q. Buat[138], D. Buchin[110], A. G. Buckley[59], M. K. Bugge[125], O. Bulekov[37], B. A. Bullard[143], S. Burdin[92], C. D. Burgard[49], A. M. Burger[40], B. Burghgrave[8], O. Burlayenko[54], J. T. P. Burr[32], C. D. Burton[11], J. C. Burzynski[142], E. L. Busch[41], V. Büscher[100], P. J. Bussey[59], J. M. Butler[25], C. M. Buttar[59], J. M. Butterworth[96], W. Buttinger[134], C. J. Buxo Vazquez[107], A. R. Buzykaev[37], G. Cabras[23b], S. Cabrera Urbán[163], L. Cadamuro[66], D. Caforio[58], H. Cai[129], Y. Cai[14a,14e], V. M. M. Cairo[36], O. Cakir[3a], N. Calace[36], P. Calafiura[17a], G. Calderini[127], P. Calfayan[68], G. Callea[59], L. P. Caloba[83b], D. Calvet[40], S. Calvet[40], T. P. Calvet[102], M. Calvetti[74a,74b], R. Camacho Toro[127], S. Camarda[36], D. Camarero Munoz[26], P. Camarri[76a,76b], M. T. Camerlingo[72a,72b], D. Cameron[125], C. Camincher[165], M. Campanelli[96], A. Camplani[42], V. Canale[72a,72b], A. Canesse[104], M. Cano Bret[80], J. Cantero[163], Y. Cao[162], F. Capocasa[26], M. Capua[43a,43b], A. Carbone[71a,71b], R. Cardarelli[76a], J. C. J. Cardenas[8], F. Cardillo[163], T. Carli[36], G. Carlino[72a], J. I. Carlotto[13], B. T. Carlson[129,v], E. M. Carlson[156a,165], L. Carminati[71a,71b], A. Carnelli[135], M. Carnesale[75a,75b], S. Caron[113], E. Carquin[137f], S. Carrá[71a,71b], G. Carratta[23a,23b], F. Carrio Argos[33g], J. W. S. Carter[155], T. M. Carter[52], M. P. Casado[13,j], M. Caspar[48], E. G. Castiglia[172], F. L. Castillo[4], L. Castillo Garcia[13], V. Castillo Gimenez[163], N. F. Castro[130a,130e], A. Catinaccio[36], J. R. Catmore[125], V. Cavaliere[29], N. Cavalli[23a,23b], V. Cavasinni[74a,74b], Y. C. Cekmecelioglu[48], E. Celebi[21a], F. Celli[126], M. S. Centonze[70a,70b], K. Cerny[122], A. S. Cerqueira[83a], A. Cerri[146], L. Cerrito[76a,76b], F. Cerutti[17a], B. Cervato[141], A. Cervelli[23b], G. Cesarini[53], S. A. Cetin[82], Z. Chadi[35a], D. Chakraborty[115], M. Chala[130f], J. Chan[170], W. Y. Chan[153], J. D. Chapman[32], E. Chapon[135], B. Chargeishvili[149b], D. G. Charlton[20], T. P. Charman[94], M. Chatterjee[19], C. Chauhan[133], S. Chekanov[6], S. V. Chekulaev[156a], G. A. Chelkov[38,a], A. Chen[106], B. Chen[151], B. Chen[165], H. Chen[14c], H. Chen[29], J. Chen[62c], J. Chen[142], M. Chen[126], S. Chen[153], S. J. Chen[14c], X. Chen[62c], X. Chen[14b,am], Y. Chen[62a], C. L. Cheng[170], H. C. Cheng[64a], S. Cheong[143], A. Cheplakov[38], E. Cheremushkina[48], E. Cherepanova[114], R. Cherkaoui El Moursli[35e], E. Cheu[7], K. Cheung[65], L. Chevalier[135], V. Chiarella[53], G. Chiarelli[74a], N. Chiedde[102], G. Chiodini[70a], A. S. Chisholm[20], A. Chitan[27b], M. Chitishvili[163], M. V. Chizhov[38], K. Choi[11], A. R. Chomont[75a,75b], Y. Chou[103], E. Y. S. Chow[114], T. Chowdhury[33g], K. L. Chu[169], M. C. Chu[64a], X. Chu[14a,14e], J. Chudoba[131], J. J. Chwastowski[87], D. Cieri[110], K. M. Ciesla[86a], V. Cindro[93], A. Ciocio[17a], F. Cirotto[72a,72b], Z. H. Citron[169,o], M. Citterio[71a], D. A. Ciubotaru[27b], B. M. Ciungu[155], A. Clark[56], P. J. Clark[52], J. M. Clavijo Columbie[48], S. E. Clawson[48], C. Clement[47a,47b], J. Clercx[48], L. Clissa[23a,23b], Y. Coadou[102], M. Cobal[69a,69c], A. Coccaro[57b], R. F. Coelho Barrue[130a], R. Coelho Lopes De Sa[103], S. Coelli[71a], H. Cohen[151], A. E. C. Coimbra[71a,71b], B. Cole[41], J. Collot[60], P. Conde Muiño[130a,130g], M. P. Connell[33c], S. H. Connell[33c], I. A. Connelly[59], E. I. Conroy[126], F. Conventi[72a,ao], H. G. Cooke[20], A. M. Cooper-Sarkar[126], A. Cordeiro Oudot Choi[127], F. Cormier[164], L. D. Corpe[40], M. Corradi[75a,75b], F. Corriveau[104,ac], A. Cortes-Gonzalez[18], M. J. Costa[163], F. Costanza[4], D. Costanzo[139], B. M. Cote[119], G. Cowan[95], K. Cranmer[170], D. Cremonini[23a,23b], S. Crépé-Renaudin[60], F. Crescioli[127], M. Cristinziani[141], M. Cristoforetti[78a,78b], V. Croft[114], J. E. Crosby[121], G. Crosetti[43a,43b], A. Cueto[99], T. Cuhadar Donszelmann[160], H. Cui[14a,14e], Z. Cui[7], W. R. Cunningham[59], F. Curcio[43a,43b], P. Czodrowski[36], M. M. Czurylo[63b], M. J. Da Cunha Sargedas De Sousa[62a], J. V. Da Fonseca Pinto[83b], C. Da Via[101], W. Dabrowski[86a], T. Dado[49], S. Dahbi[33g], T. Dai[106], C. Dallapiccola[103], M. Dam[42], G. D'amen[29], V. D'Amico[109], J. Damp[100], J. R. Dandoy[128], M. F. Daneri[30], M. Danninger[142], V. Dao[36], G. Darbo[57b], S. Darmora[6], S. J. Das[29,ap], S. D'Auria[71a,71b], C. David[156b], T. Davidek[133], B. Davis-Purcell[34], I. Dawson[94], H. A. Day-hall[132], K. De[8], R. De Asmundis[72a], N. De Biase[48], S. De Castro[23a,23b], N. De Groot[113], P. de Jong[114], H. De la Torre[107], A. De Maria[14c], A. De Salvo[75a], U. De Sanctis[76a,76b], A. De Santo[146], J. B. De Vivie De Regie[60], D. V. Dedovich[38], J. Degens[114], A. M. Deiana[44], F. Del Corso[23a,23b], J. Del Peso[99], F. Del Rio[63a], F. Deliot[135], C. M. Delitzsch[49], M. Della Pietra[72a,72b], D. Della Volpe[56], A. Dell'Acqua[36], L. Dell'Asta[71a,71b], M. Delmastro[4], P. A. Delsart[60], S. Demers[172], M. Demichev[38], S. P. Denisov[37], L. D'Eramo[40], D. Derendarz[87], F. Derue[127], P. Dervan[92], K. Desch[24], C. Deutsch[24], F. A. Di Bello[57a,57b], A. Di Ciaccio[76a,76b], L. Di Ciaccio[4], A. Di Domenico[75a,75b], C. Di Donato[72a,72b], A. Di Girolamo[36], G. Di Gregorio[5], A. Di Luca[78a,78b], B. Di Micco[77a,77b], R. Di Nardo[77a,77b], C. Diaconu[102], M. Diamantopoulou[34], F. A. Dias[114], T. Dias Do Vale[142], M. A. Diaz[137a,137b], F. G. Diaz Capriles[24], M. Didenko[163], E. B. Diehl[106], L. Diehl[54], S. Díez Cornell[48], C. Diez Pardos[141],

C. Dimitriadi[24,161], A. Dimitrievska[17a], J. Dingfelder[24], I.-M. Dinu[27b], S. J. Dittmeier[63b], F. Dittus[36], F. Djama[102], T. Djobava[149b], J. I. Djuvsland[16], C. Doglioni[98,101], J. Dolejsi[133], Z. Dolezal[133], M. Donadelli[83c], B. Dong[107], J. Donini[40], A. D'Onofrio[77a,77b], M. D'Onofrio[92], J. Dopke[134], A. Doria[72a], N. Dos Santos Fernandes[130a], M. T. Dova[90], A. T. Doyle[59], M. A. Draguet[126], E. Dreyer[169], I. Drivas-koulouris[10], A. S. Drobac[158], M. Drozdova[56], D. Du[62a], T. A. du Pree[114], F. Dubinin[37], M. Dubovsky[28a], E. Duchovni[169], G. Duckeck[109], O. A. Ducu[27b], D. Duda[52], A. Dudarev[36], E. R. Duden[26], M. D'uffizi[101], L. Duflot[66], M. Dührssen[36], C. Dülsen[171], A. E. Dumitriu[27b], M. Dunford[63a], S. Dungs[49], K. Dunne[47a,47b], A. Duperrin[102], H. Duran Yildiz[3a], M. Düren[58], A. Durglishvili[149b], B. L. Dwyer[115], G. I. Dyckes[17a], M. Dyndal[86a], S. Dysch[101], B. S. Dziedzic[87], Z. O. Earnshaw[146], G. H. Eberwein[126], B. Eckerova[28a], S. Eggebrecht[55], M. G. Eggleston[51], E. Egidio Purcino De Souza[127], L. F. Ehrke[56], G. Eigen[16], K. Einsweiler[17a], T. Ekelof[161], P. A. Ekman[98], S. El Farkh[35b], Y. El Ghazali[35b], H. El Jarrari[35e,148], A. El Moussaouy[35a], V. Ellajosyula[161], M. Ellert[161], F. Ellinghaus[171], A. A. Elliot[94], N. Ellis[36], J. Elmsheuser[29], M. Elsing[36], D. Emeliyanov[134], Y. Enari[153], I. Ene[17a], S. Epari[13], J. Erdmann[49], P. A. Erland[87], M. Errenst[171], M. Escalier[66], C. Escobar[163], E. Etzion[151], G. Evans[130a], H. Evans[68], L. S. Evans[95], M. O. Evans[146], A. Ezhilov[37], S. Ezzarqtouni[35a], F. Fabbri[59], L. Fabbri[23a,23b], G. Facini[96], V. Fadeyev[136], R. M. Fakhrutdinov[37], S. Falciano[75a], L. F. Falda Ulhoa Coelho[36], P. J. Falke[24], J. Faltova[133], C. Fan[162], Y. Fan[14a], Y. Fang[14a,14e], M. Fanti[71a,71b], M. Faraj[69a,69b], Z. Farazpay[97], A. Farbin[8], A. Farilla[77a], T. Farooque[107], S. M. Farrington[52], F. Fassi[35e], D. Fassouliotis[9], M. Faucci Giannelli[76a,76b], W. J. Fawcett[32], L. Fayard[66], P. Federic[133], P. Federicova[131], O. L. Fedin[37,a], G. Fedotov[37], M. Feickert[170], L. Feligioni[102], D. E. Fellers[123], C. Feng[62b], M. Feng[14b], Z. Feng[114], M. J. Fenton[160], A. B. Fenyuk[37], L. Ferencz[48], R. A. M. Ferguson[91], S. I. Fernandez Luengo[137f], M. J. V. Fernoux[102], J. Ferrando[48], A. Ferrari[161], P. Ferrari[113,114], R. Ferrari[73a], D. Ferrere[56], C. Ferretti[106], F. Fiedler[100], A. Filipčič[93], E. K. Filmer[1], F. Filthaut[113], M. C. N. Fiolhais[130a,130c,d], L. Fiorini[163], W. C. Fisher[107], T. Fitschen[101], P. M. Fitzhugh[135], I. Fleck[141], P. Fleischmann[106], T. Flick[171], L. Flores[128], M. Flores[33d,aj], L. R. Flores Castillo[64a], L. Flores Sanz De Acedo[36], F. M. Follega[78a,78b], N. Fomin[16], J. H. Foo[155], B. C. Forland[68], A. Formica[135], A. C. Forti[101], E. Fortin[36], A. W. Fortman[61], M. G. Foti[17a], L. Fountas[9,k], D. Fournier[66], H. Fox[91], P. Francavilla[74a,74b], S. Francescato[61], S. Franchellucci[56], M. Franchini[23a,23b], S. Franchino[63a], D. Francis[36], L. Franco[113], L. Franconi[48], M. Franklin[61], G. Frattari[26], A. C. Freegard[94], W. S. Freund[83b], Y. Y. Frid[151], N. Fritzsche[50], A. Froch[54], D. Froidevaux[36], J. A. Frost[126], Y. Fu[62a], M. Fujimoto[118], E. Fullana Torregrosa[163,*], K. Y. Fung[64a], E. Furtado De Simas Filho[83b], M. Furukawa[153], J. Fuster[163], A. Gabrielli[23a,23b], A. Gabrielli[155], P. Gadow[36], G. Gagliardi[57a,57b], L. G. Gagnon[17a], E. J. Gallas[126], B. J. Gallop[134], K. K. Gan[119], S. Ganguly[153], J. Gao[62a], Y. Gao[52], F. M. Garay Walls[137a,137b], B. Garcia[29,ap], C. García[163], A. Garcia Alonso[114], A. G. Garcia Caffaro[172], J. E. García Navarro[163], M. Garcia-Sciveres[17a], G. L. Gardner[128], R. W. Gardner[39], N. Garelli[158], D. Garg[80], R. B. Garg[143,s], J. M. Gargan[52], C. A. Garner[155], S. J. Gasiorowski[138], P. Gaspar[83b], G. Gaudio[73a], V. Gautam[13], P. Gauzzi[75a,75b], I. L. Gavrilenko[37], A. Gavrilyuk[37], C. Gay[164], G. Gaycken[48], E. N. Gazis[10], A. A. Geanta[27b], C. M. Gee[136], C. Gemme[57b], M. H. Genest[60], S. Gentile[75a,75b], S. George[95], W. F. George[20], T. Geralis[46], P. Gessinger-Befurt[36], M. E. Geyik[171], M. Ghneimat[141], K. Ghorbanian[94], A. Ghosal[141], A. Ghosh[160], A. Ghosh[7], B. Giacobbe[23b], S. Giagu[75a,75b], P. Giannetti[74a], A. Giannini[62a], S. M. Gibson[95], M. Gignac[136], D. T. Gil[86b], A. K. Gilbert[86a], B. J. Gilbert[41], D. Gillberg[34], G. Gilles[114], N. E. K. Gillwald[48], L. Ginabat[127], D. M. Gingrich[2,an], M. P. Giordani[69a,69c], P. F. Giraud[135], G. Giugliarelli[69a,69c], D. Giugni[71a], F. Giuli[36], I. Gkialas[9,k], L. K. Gladilin[37], C. Glasman[99], G. R. Gledhill[123], G. Glemža[48], M. Glisic[123], I. Gnesi[43b,g], Y. Go[29,ap], M. Goblirsch-Kolb[36], B. Gocke[49], D. Godin[108], B. Gokturk[21a], S. Goldfarb[105], T. Golling[56], M. G. D. Gololo[33g], D. Golubkov[37], J. P. Gombas[107], A. Gomes[130a,130b], G. Gomes Da Silva[141], A. J. Gomez Delegido[163], R. Gonçalo[130a,130c], G. Gonella[123], L. Gonella[20], A. Gongadze[149c], F. Gonnella[20], J. L. Gonski[41], R. Y. González Andana[52], S. González de la Hoz[163], S. Gonzalez Fernandez[13], R. Gonzalez Lopez[92], C. Gonzalez Renteria[17a], R. Gonzalez Suarez[161], S. Gonzalez-Sevilla[56], G. R. Gonzalvo Rodriguez[163], L. Goossens[36], P. A. Gorbounov[37], B. Gorini[36], E. Gorini[70a,70b], A. Gorišek[93], T. C. Gosart[128], A. T. Goshaw[51], M. I. Gostkin[38], S. Goswami[121], C. A. Gottardo[36], M. Gouighri[35b], V. Goumarre[48], A. G. Goussiou[138], N. Govender[33c], I. Grabowska-Bold[86a], K. Graham[34], E. Gramstad[125], S. Grancagnolo[70a,70b], M. Grandi[146], P. M. Gravila[27f], F. G. Gravili[70a,70b], H. M. Gray[17a], M. Greco[70a,70b], C. Grefe[24], I. M. Gregor[48], P. Grenier[143], C. Grieco[13], A. A. Grillo[136], K. Grimm[31], S. Grinstein[13,y], J.-F. Grivaz[66], E. Gross[169], J. Grosse-Knetter[55], C. Grud[106], J. C. Grundy[126],

L. Guan[106], W. Guan[29], C. Gubbels[164], J. G. R. Guerrero Rojas[163], G. Guerrieri[69a,69c], F. Guescini[110], R. Gugel[100], J. A. M. Guhit[106], A. Guida[18], T. Guillemin[4], E. Guilloton[134,167], S. Guindon[36], F. Guo[14a,14e], J. Guo[62c], L. Guo[48], Y. Guo[106], R. Gupta[48], S. Gurbuz[24], S. S. Gurdasani[54], G. Gustavino[36], M. Guth[56], P. Gutierrez[120], L. F. Gutierrez Zagazeta[128], C. Gutschow[96], C. Gwenlan[126], C. B. Gwilliam[92], E. S. Haaland[125], A. Haas[117], M. Habedank[48], C. Haber[17a], H. K. Hadavand[8], A. Hadef[100], S. Hadzic[110], J. J. Hahn[141], E. H. Haines[96], M. Haleem[166], J. Haley[121], J. J. Hall[139], G. D. Hallewell[102], L. Halser[19], K. Hamano[165], H. Hamdaoui[35e], M. Hamer[24], G. N. Hamity[52], E. J. Hampshire[95], J. Han[62b], K. Han[62a], L. Han[14c], L. Han[62a], S. Han[17a], Y. F. Han[155], K. Hanagaki[84], M. Hance[136], D. A. Hangal[41,ai], H. Hanif[142], M. D. Hank[128], R. Hankache[101], J. B. Hansen[42], J. D. Hansen[42], P. H. Hansen[42], K. Hara[157], D. Harada[56], T. Harenberg[171], S. Harkusha[37], M. L. Harris[103], Y. T. Harris[126], J. Harrison[13], N. M. Harrison[119], P. F. Harrison[167], N. M. Hartman[110], N. M. Hartmann[109], Y. Hasegawa[140], A. Hasib[52], S. Haug[19], R. Hauser[107], C. M. Hawkes[20], R. J. Hawkings[36], Y. Hayashi[153], S. Hayashida[111], D. Hayden[107], C. Hayes[106], R. L. Hayes[114], C. P. Hays[126], J. M. Hays[94], H. S. Hayward[92], F. He[62a], M. He[14a,14e], Y. He[154], Y. He[127], N. B. Heatley[94], V. Hedberg[98], A. L. Heggelund[125], N. D. Hehir[94], C. Heidegger[54], K. K. Heidegger[54], W. D. Heidorn[81], J. Heilman[34], S. Heim[48], T. Heim[17a], J. G. Heinlein[128], J. J. Heinrich[123], L. Heinrich[110,al], J. Hejbal[131], L. Helary[48], A. Held[170], S. Hellesund[16], C. M. Helling[164], S. Hellman[47a,47b], R. C. W. Henderson[91], L. Henkelmann[32], A. M. Henriques Correia[36], H. Herde[98], Y. Hernández Jiménez[145], L. M. Herrmann[24], T. Herrmann[50], G. Herten[54], R. Hertenberger[109], L. Hervas[36], M. E. Hesping[100], N. P. Hessey[156a], H. Hibi[85], S. J. Hillier[20], J. R. Hinds[107], F. Hinterkeuser[24], M. Hirose[124], S. Hirose[157], D. Hirschbuehl[171], T. G. Hitchings[101], B. Hiti[93], J. Hobbs[145], R. Hobincu[27e], N. Hod[169], M. C. Hodgkinson[139], B. H. Hodkinson[32], A. Hoecker[36], J. Hofer[48], T. Holm[24], M. Holzbock[110], L. B. A. H. Hommels[32], B. P. Honan[101], J. Hong[62c], T. M. Hong[129], B. H. Hooberman[162], W. H. Hopkins[6], Y. Horii[111], S. Hou[148], A. S. Howard[93], J. Howarth[59], J. Hoya[6], M. Hrabovsky[122], A. Hrynevich[48], T. Hryn'ova[4], P. J. Hsu[65], S. -C. Hsu[138], Q. Hu[41], Y. F. Hu[14a,14e], S. Huang[64b], X. Huang[14c], Y. Huang[139,m], Y. Huang[14a], Z. Huang[101], Z. Hubacek[132], M. Huebner[24], F. Huegging[24], T. B. Huffman[126], C. A. Hugli[48], M. Huhtinen[36], S. K. Huiberts[16], R. Hulsken[104], N. Huseynov[12,a], J. Huston[107], J. Huth[61], R. Hyneman[143], G. Iacobucci[56], G. Iakovidis[29], I. Ibragimov[141], L. Iconomidou-Fayard[66], P. Iengo[72a,72b], R. Iguchi[153], T. Iizawa[84], Y. Ikegami[84], N. Ilic[155], H. Imam[35a], M. Ince Lezki[56], T. Ingebretsen Carlson[47a,47b], G. Introzzi[73a,73b], M. Iodice[77a], V. Ippolito[75a,75b], R. K. Irwin[92], M. Ishino[153], W. Islam[170], C. Issever[18,48], S. Istin[21a,ar], H. Ito[168], J. M. Iturbe Ponce[64a], R. Iuppa[78a,78b], A. Ivina[169], J. M. Izen[45], V. Izzo[72a], P. Jacka[131,132], P. Jackson[1], R. M. Jacobs[48], B. P. Jaeger[142], C. S. Jagfeld[109], P. Jain[54], G. Jäkel[171], K. Jakobs[54], T. Jakoubek[169], J. Jamieson[59], K. W. Janas[86a], A. E. Jaspan[92], M. Javurkova[103], F. Jeanneau[135], L. Jeanty[123], J. Jejelava[149a,af], P. Jenni[54,h], C. E. Jessiman[34], S. Jézéquel[4], C. Jia[62b], J. Jia[145], X. Jia[61], X. Jia[14a,14e], Z. Jia[14c], Y. Jiang[62a], S. Jiggins[48], J. Jimenez Pena[13], S. Jin[14c], A. Jinaru[27b], O. Jinnouchi[154], P. Johansson[139], K. A. Johns[7], J. W. Johnson[136], D. M. Jones[32], E. Jones[48], P. Jones[32], R. W. L. Jones[91], T. J. Jones[92], R. Joshi[119], J. Jovicevic[15], X. Ju[17a], J. J. Junggeburth[36], T. Junkermann[63a], A. Juste Rozas[13,y], M. K. Juzek[87], S. Kabana[137e], A. Kaczmarska[87], M. Kado[110], H. Kagan[119], M. Kagan[143], A. Kahn[41], A. Kahn[128], C. Kahra[100], T. Kaji[168], E. Kajomovitz[150], N. Kakati[169], I. Kalaitzidou[54], C. W. Kalderon[29], A. Kamenshchikov[155], S. Kanayama[154], N. J. Kang[136], D. Kar[33g], K. Karava[126], M. J. Kareem[156b], E. Karentzos[54], I. Karkanias[152], O. Karkout[114], S. N. Karpov[38], Z. M. Karpova[38], V. Kartvelishvili[91], A. N. Karyukhin[37], E. Kasimi[152], J. Katzy[48], S. Kaur[34], K. Kawade[140], M. P. Kawale[120], T. Kawamoto[135], E. F. Kay[36], F. I. Kaya[158], S. Kazakos[107], V. F. Kazanin[37], Y. Ke[145], J. M. Keaveney[33a], R. Keeler[165], G. V. Kehris[61], J. S. Keller[34], A. S. Kelly[96], J. J. Kempster[146], K. E. Kennedy[41], P. D. Kennedy[100], O. Kepka[131], B. P. Kerridge[167], S. Kersten[171], B. P. Kerševan[93], S. Keshri[66], L. Keszeghova[28a], S. Ketabchi Haghighat[155], M. Khandoga[127], A. Khanov[121], A. G. Kharlamov[37], T. Kharlamova[37], E. E. Khoda[138], T. J. Khoo[18], G. Khoriauli[166], J. Khubua[149b], Y. A. R. Khwaira[66], A. Kilgallon[123], D. W. Kim[47a,47b], Y. K. Kim[39], N. Kimura[96], A. Kirchhoff[55], C. Kirfel[24], F. Kirfel[24], J. Kirk[134], A. E. Kiryunin[110], C. Kitsaki[10], O. Kivernyk[24], M. Klassen[63a], C. Klein[34], L. Klein[166], M. H. Klein[106], M. Klein[92], S. B. Klein[56], U. Klein[92], P. Klimek[36], A. Klimentov[29], T. Klioutchnikova[36], P. Kluit[114], S. Kluth[110], E. Kneringer[79], T. M. Knight[155], A. Knue[54], R. Kobayashi[88], S. F. Koch[126], M. Kocian[143], P. Kodyš[133], D. M. Koeck[123], P. T. Koenig[24], T. Koffas[34], M. Kolb[135], I. Koletsou[4], T. Komarek[122], K. Köneke[54], A. X. Y. Kong[1], T. Kono[118], N. Konstantinidis[96], B. Konya[98], R. Kopeliansky[68], S. Koperny[86a], K. Korcyl[87], K. Kordas[152,f], G. Koren[151], A. Korn[96],

S. Korn[55], I. Korolkov[13], N. Korotkova[37], B. Kortman[114], O. Kortner[110], S. Kortner[110], W. H. Kostecka[115], V. V. Kostyukhin[141], A. Kotsokechagia[135], A. Kotwal[51], A. Koulouris[36], A. Kourkoumeli-Charalampidi[73a,73b], C. Kourkoumelis[9], E. Kourlitis[110,al], O. Kovanda[146], R. Kowalewski[165], W. Kozanecki[135], A. S. Kozhin[37], V. A. Kramarenko[37], G. Kramberger[93], P. Kramer[100], M. W. Krasny[127], A. Krasznahorkay[36], J. W. Kraus[171], J. A. Kremer[100], T. Kresse[50], J. Kretzschmar[92], K. Kreul[18], P. Krieger[155], S. Krishnamurthy[103], M. Krivos[133], K. Krizka[20], K. Kroeninger[49], H. Kroha[110], J. Kroll[131], J. Kroll[128], K. S. Krowpman[107], U. Kruchonak[38], H. Krüger[24], N. Krumnack[81], M. C. Kruse[51], J. A. Krzysiak[87], O. Kuchinskaia[37], S. Kuday[3a], S. Kuehn[36], R. Kuesters[54], T. Kuhl[48], V. Kukhtin[38], Y. Kulchitsky[37,a], S. Kuleshov[137b,137d], M. Kumar[33g], N. Kumari[102], A. Kupco[131], T. Kupfer[49], A. Kupich[37], O. Kuprash[54], H. Kurashige[85], L. L. Kurchaninov[156a], O. Kurdysh[66], Y. A. Kurochkin[37], A. Kurova[37], M. Kuze[154], A. K. Kvam[103], J. Kvita[122], T. Kwan[104], N. G. Kyriacou[106], L. A. O. Laatu[102], C. Lacasta[163], F. Lacava[75a,75b], H. Lacker[18], D. Lacour[127], N. N. Lad[96], E. Ladygin[38], B. Laforge[127], T. Lagouri[137e], S. Lai[55], I. K. Lakomiec[86a], N. Lalloue[60], J. E. Lambert[165,n], S. Lammers[68], W. Lampl[7], C. Lampoudis[152,f], A. N. Lancaster[115], E. Lançon[29], U. Landgraf[54], M. P. J. Landon[94], V. S. Lang[54], R. J. Langenberg[103], O. K. B. Langrekken[125], A. J. Lankford[160], F. Lanni[36], K. Lantzsch[24], A. Lanza[73a], A. Lapertosa[57a,57b], J. F. Laporte[135], T. Lari[71a], F. Lasagni Manghi[23b], M. Lassnig[36], V. Latonova[131], A. Laudrain[100], A. Laurier[150], S. D. Lawlor[95], Z. Lawrence[101], M. Lazzaroni[71a,71b], B. Le[101], E. M. Le Boulicaut[51], B. Leban[93], A. Lebedev[81], M. LeBlanc[36], F. Ledroit-Guillon[60], A. C. A. Lee[96], S. C. Lee[148], S. Lee[47a,47b], T. F. Lee[92], L. L. Leeuw[33c], H. P. Lefebvre[95], M. Lefebvre[165], C. Leggett[17a], G. Lehmann Miotto[36], M. Leigh[56], W. A. Leight[103], W. Leinonen[113], A. Leisos[152,x], M. A. L. Leite[83c], C. E. Leitgeb[48], R. Leitner[133], K. J. C. Leney[44], T. Lenz[24], S. Leone[74a], C. Leonidopoulos[52], A. Leopold[144], C. Leroy[108], R. Les[107], C. G. Lester[32], M. Levchenko[37], J. Levêque[4], D. Levin[106], L. J. Levinson[169], M. P. Lewicki[87], D. J. Lewis[4], A. Li[5], B. Li[62b], C. Li[62a], C.-Q. Li[62c], H. Li[62a], H. Li[62b], H. Li[14c], H. Li[62b], K. Li[138], L. Li[62c], M. Li[14a,14e], Q. Y. Li[62a], S. Li[14a,14e], S. Li[62d,62c,e], T. Li[5,c], X. Li[104], Z. Li[126], Z. Li[104], Z. Li[92], Z. Li[14a,14e], Z. Liang[14a], M. Liberatore[135,ag], B. Liberti[76a], K. Lie[64c], J. Lieber Marin[83b], H. Lien[68], K. Lin[107], R. E. Lindley[7], J. H. Lindon[2], A. Linss[48], E. Lipeles[128], A. Lipniacka[16], A. Lister[164], J. D. Little[4], B. Liu[14a], B. X. Liu[142], D. Liu[62c,62d], J. B. Liu[62a], J. K. K. Liu[32], K. Liu[62c,62d], M. Liu[62a], M. Y. Liu[62a], P. Liu[14a], Q. Liu[62c,62d,138], X. Liu[62a], Y. Liu[14d,14e], Y. L. Liu[106], Y. W. Liu[62a], J. Llorente Merino[142], S. L. Lloyd[94], E. M. Lobodzinska[48], P. Loch[7], S. Loffredo[76a,76b], T. Lohse[18], K. Lohwasser[139], E. Loiacono[48], M. Lokajicek[131,*], J. D. Lomas[20], J. D. Long[162], I. Longarini[160], L. Longo[70a,70b], R. Longo[162], I. Lopez Paz[67], A. Lopez Solis[48], J. Lorenz[109], N. Lorenzo Martinez[4], A. M. Lory[109], O. Loseva[37], X. Lou[47a,47b], X. Lou[14a,14e], A. Lounis[66], J. Love[6], P. A. Love[91], G. Lu[14a,14e], M. Lu[80], S. Lu[128], Y. J. Lu[65], H. J. Lubatti[138], C. Luci[75a,75b], F. L. Lucio Alves[14c], A. Lucotte[60], F. Luehring[68], I. Luise[145], O. Lukianchuk[66], O. Lundberg[144], B. Lund-Jensen[144], N. A. Luongo[123], M. S. Lutz[151], D. Lynn[29], H. Lyons[92], R. Lysak[131], E. Lytken[98], V. Lyubushkin[38], T. Lyubushkina[38], M. M. Lyukova[145], H. Ma[29], K. Ma[62a], L. L. Ma[62b], Y. Ma[121], D. M. Mac Donell[165], G. Maccarrone[53], J. C. MacDonald[100], R. Madar[40], W. F. Mader[50], J. Maeda[85], T. Maeno[29], M. Maerker[50], H. Maguire[139], V. Maiboroda[135], A. Maio[130a,130b,130d], K. Maj[86a], O. Majersky[48], S. Majewski[123], N. Makovec[66], V. Maksimovic[15], B. Malaescu[127], Pa. Malecki[87], V. P. Maleev[37], F. Malek[60], M. Mali[93], D. Malito[95,r], U. Mallik[80], S. Maltezos[10], S. Malyukov[38], J. Mamuzic[13], G. Mancini[53], G. Manco[73a,73b], J. P. Mandalia[94], I. Mandić[93], L. Manhaes de Andrade Filho[83a], I. M. Maniatis[169], J. Manjarres Ramos[102,ah], D. C. Mankad[169], A. Mann[109], B. Mansoulie[135], S. Manzoni[36], A. Marantis[152,x], G. Marchiori[5], M. Marcisovsky[131], C. Marcon[71a,71b], M. Marinescu[20], M. Marjanovic[120], E. J. Marshall[91], Z. Marshall[17a], S. Marti-Garcia[163], T. A. Martin[167], V. J. Martin[52], B. Martin dit Latour[16], L. Martinelli[75a,75b], M. Martinez[13,y], P. Martinez Agullo[163], V. I. Martinez Outschoorn[103], P. Martinez Suarez[13], S. Martin-Haugh[134], V. S. Martoiu[27b], A. C. Martyniuk[96], A. Marzin[36], D. Mascione[78a,78b], L. Masetti[100], T. Mashimo[153], J. Masik[101], A. L. Maslennikov[37], L. Massa[23b], P. Massarotti[72a,72b], P. Mastrandrea[74a,74b], A. Mastroberardino[43a,43b], T. Masubuchi[153], T. Mathisen[161], J. Matousek[133], N. Matsuzawa[153], J. Maurer[27b], B. Maček[93], D. A. Maximov[37], R. Mazini[148], I. Maznas[152], M. Mazza[107], S. M. Mazza[136], E. Mazzeo[71a,71b], C. Mc Ginn[29], J. P. Mc Gowan[104], S. P. Mc Kee[106], E. F. McDonald[105], A. E. McDougall[114], J. A. Mcfayden[146], R. P. McGovern[128], G. Mchedlidze[149b], R. P. Mckenzie[33g], T. C. Mclachlan[48], D. J. Mclaughlin[96], K. D. McLean[165], S. J. McMahon[134], P. C. McNamara[105], C. M. Mcpartland[92], R. A. McPherson[165,ac], S. Mehlhase[109], A. Mehta[92], D. Melini[150], B. R. Mellado Garcia[33g], A. H. Melo[55], F. Meloni[48],

A. M. Mendes Jacques Da Costa[101], H. Y. Meng[155], L. Meng[91], S. Menke[110], M. Mentink[36], E. Meoni[43a,43b], C. Merlassino[126], L. Merola[72a,72b], C. Meroni[71a,71b], G. Merz[106], O. Meshkov[37], J. Metcalfe[6], A. S. Mete[6], C. Meyer[68], J.-P. Meyer[135], R. P. Middleton[134], L. Mijović[52], G. Mikenberg[169], M. Mikestikova[131], M. Mikuž[93], H. Mildner[100], A. Milic[36], C. D. Milke[44], D. W. Miller[39], L. S. Miller[34], A. Milov[169], D. A. Milstead[47a,47b], T. Min[14c], A. A. Minaenko[37], I. A. Minashvili[149b], L. Mince[59], A. I. Mincer[117], B. Mindur[86a], M. Mineev[38], Y. Mino[88], L. M. Mir[13], M. Miralles Lopez[163], M. Mironova[17a], A. Mishima[153], M. C. Missio[113], T. Mitani[168], A. Mitra[167], V. A. Mitsou[163], O. Miu[155], P. S. Miyagawa[94], Y. Miyazaki[89], A. Mizukami[84], T. Mkrtchyan[63a], M. Mlinarevic[96], T. Mlinarevic[96], M. Mlynarikova[36], S. Mobius[19], K. Mochizuki[108], P. Moder[48], P. Mogg[109], A. F. Mohammed[14a,14e], S. Mohapatra[41], G. Mokgatitswane[33g], L. Moleri[169], B. Mondal[141], S. Mondal[132], G. Monig[146], K. Mönig[48], E. Monnier[102], L. Monsonis Romero[163], J. Montejo Berlingen[13,84], M. Montella[119], F. Montereali[77a,77b], F. Monticelli[90], S. Monzani[69a,69c], N. Morange[66], A. L. Moreira De Carvalho[130a], M. Moreno Llácer[163], C. Moreno Martinez[56], P. Morettini[57b], S. Morgenstern[36], M. Morii[61], M. Morinaga[153], A. K. Morley[36], F. Morodei[75a,75b], L. Morvaj[36], P. Moschovakos[36], B. Moser[36], M. Mosidze[149b], T. Moskalets[54], P. Moskvitina[113], J. Moss[31,p], E. J. W. Moyse[103], O. Mtintsilana[33g], S. Muanza[102], J. Mueller[129], D. Muenstermann[91], R. Müller[19], G. A. Mullier[161], A. J. Mullin[32], J. J. Mullin[128], D. P. Mungo[155], D. Munoz Perez[163], F. J. Munoz Sanchez[101], M. Murin[101], W. J. Murray[134,167], A. Murrone[71a,71b], J. M. Muse[120], M. Muškinja[17a], C. Mwewa[29], A. G. Myagkov[37,a], A. J. Myers[8], A. A. Myers[129], G. Myers[68], M. Myska[132], B. P. Nachman[17a], O. Nackenhorst[49], A. Nag[50], K. Nagai[126], K. Nagano[84], J. L. Nagle[29,ap], E. Nagy[102], A. M. Nairz[36], Y. Nakahama[84], K. Nakamura[84], K. Nakkalil[5], H. Nanjo[124], R. Narayan[44], E. A. Narayanan[112], I. Naryshkin[37], M. Naseri[34], S. Nasri[159], C. Nass[24], G. Navarro[22a], J. Navarro-Gonzalez[163], R. Nayak[151], A. Nayaz[18], P. Y. Nechaeva[37], F. Nechansky[48], L. Nedic[126], T. J. Neep[20], A. Negri[73a,73b], M. Negrini[23b], C. Nellist[114], C. Nelson[104], K. Nelson[106], S. Nemecek[131], M. Nessi[36,i], M. S. Neubauer[162], F. Neuhaus[100], J. Neundorf[48], R. Newhouse[164], P. R. Newman[20], C. W. Ng[129], Y. W. Y. Ng[48], B. Ngair[35e], H. D. N. Nguyen[108], R. B. Nickerson[126], R. Nicolaidou[135], J. Nielsen[136], M. Niemeyer[55], J. Niermann[36,55], N. Nikiforou[36], V. Nikolaenko[37,a], I. Nikolic-Audit[127], K. Nikolopoulos[20], P. Nilsson[29], I. Ninca[48], H. R. Nindhito[56], G. Ninio[151], A. Nisati[75a], N. Nishu[2], R. Nisius[110], J.-E. Nitschke[50], E. K. Nkadimeng[33g], S. J. Noacco Rosende[90], T. Nobe[153], D. L. Noel[32], T. Nommensen[147], M. B. Norfolk[139], R. R. B. Norisam[96], B. J. Norman[34], J. Novak[93], T. Novak[48], L. Novotny[132], R. Novotny[112], L. Nozka[122], K. Ntekas[160], N. M. J. Nunes De Moura Junior[83b], E. Nurse[96], J. Ocariz[127], A. Ochi[85], I. Ochoa[130a], S. Oerdek[161], J. T. Offermann[39], A. Ogrodnik[133], A. Oh[101], C. C. Ohm[144], H. Oide[84], R. Oishi[153], M. L. Ojeda[48], Y. Okazaki[88], M. W. O'Keefe[92], Y. Okumura[153], L. F. Oleiro Seabra[130a], S. A. Olivares Pino[137d], D. Oliveira Damazio[29], D. Oliveira Goncalves[83a], J. L. Oliver[160], A. Olszewski[87], Ö. O. Öncel[54], D. C. O'Neil[142], A. P. O'Neill[19], A. Onofre[130a,130e], P. U. E. Onyisi[11], M. J. Oreglia[39], G. E. Orellana[90], D. Orestano[77a,77b], N. Orlando[13], R. S. Orr[155], V. O'Shea[59], L. M. Osojnak[128], R. Ospanov[62a], G. Otero y Garzon[30], H. Otono[89], P. S. Ott[63a], G. J. Ottino[17a], M. Ouchrif[35d], J. Ouellette[29], F. Ould-Saada[125], M. Owen[59], R. E. Owen[134], K. Y. Oyulmaz[21a], V. E. Ozcan[21a], N. Ozturk[8], S. Ozturk[82], H. A. Pacey[32], A. Pacheco Pages[13], C. Padilla Aranda[13], G. Padovano[75a,75b], S. Pagan Griso[17a], G. Palacino[68], A. Palazzo[70a,70b], S. Palestini[36], J. Pan[172], T. Pan[64a], D. K. Panchal[11], C. E. Pandini[114], J. G. Panduro Vazquez[95], H. Pang[14b], P. Pani[48], G. Panizzo[69a,69c], L. Paolozzi[56], C. Papadatos[108], S. Parajuli[44], A. Paramonov[6], C. Paraskevopoulos[10], D. Paredes Hernandez[64b], T. H. Park[155], M. A. Parker[32], F. Parodi[57a,57b], E. W. Parrish[115], V. A. Parrish[52], J. A. Parsons[41], U. Parzefall[54], B. Pascual Dias[108], L. Pascual Dominguez[151], F. Pasquali[114], E. Pasqualucci[75a], S. Passaggio[57b], F. Pastore[95], P. Pasuwan[47a,47b], P. Patel[87], U. M. Patel[51], J. R. Pater[101], T. Pauly[36], J. Pearkes[143], M. Pedersen[125], R. Pedro[130a], S. V. Peleganchuk[37], O. Penc[36], E. A. Pender[52], H. Peng[62a], K. E. Penski[109], M. Penzin[37], B. S. Peralva[83d], A. P. Pereira Peixoto[60], L. Pereira Sanchez[47a,47b], D. V. Perepelitsa[29,ap], E. Perez Codina[156a], M. Perganti[10], L. Perini[71a,71b,*], H. Pernegger[36], O. Perrin[40], K. Peters[48], R. F. Y. Peters[101], B. A. Petersen[36], T. C. Petersen[42], E. Petit[102], V. Petousis[132], C. Petridou[152,f], A. Petrukhin[141], M. Pettee[17a], N. E. Pettersson[36], A. Petukhov[37], K. Petukhova[133], A. Peyaud[135], R. Pezoa[137f], L. Pezzotti[36], G. Pezzullo[172], T. M. Pham[170], T. Pham[105], P. W. Phillips[134], G. Piacquadio[145], E. Pianori[17a], F. Piazza[71a,71b], R. Piegaia[30], D. Pietreanu[27b], A. D. Pilkington[101], M. Pinamonti[69a,69c], J. L. Pinfold[2], B. C. Pinheiro Pereira[130a], A. E. Pinto Pinoargote[135], K. M. Piper[146], A. Pirttikoski[56], C. Pitman Donaldson[96], D. A. Pizzi[34], L. Pizzimento[64b], A. Pizzini[114], M. -A. Pleier[29],

V. Plesanovs[54], V. Pleskot[133], E. Plotnikova[38], G. Poddar[4], R. Poettgen[98], L. Poggioli[127], I. Pokharel[55], S. Polacek[133], G. Polesello[73a], A. Poley[142,156a], R. Polifka[132], A. Polini[23b], C. S. Pollard[167], Z. B. Pollock[119], V. Polychronakos[29], E. Pompa Pacchi[75a,75b], D. Ponomarenko[113], L. Pontecorvo[36], S. Popa[27a], G. A. Popeneciu[27d], A. Poreba[36], D. M. Portillo Quintero[156a], S. Pospisil[132], M. A. Postill[139], P. Postolache[27c], K. Potamianos[167], P. A. Potepa[86a], I. N. Potrap[38], C. J. Potter[32], H. Potti[1], T. Poulsen[48], J. Poveda[163], M. E. Pozo Astigarraga[36], A. Prades Ibanez[163], J. Pretel[54], D. Price[101], M. Primavera[70a], M. A. Principe Martin[99], R. Privara[122], T. Procter[59], M. L. Proffitt[138], N. Proklova[128], K. Prokofiev[64c], G. Proto[110], S. Protopopescu[29], J. Proudfoot[6], M. Przybycien[86a], W. W. Przygoda[86b], J. E. Puddefoot[139], D. Pudzha[37], D. Pyatiizbyantseva[37], J. Qian[106], D. Qichen[101], Y. Qin[101], T. Qiu[52], A. Quadt[55], M. Queitsch-Maitland[101], G. Quetant[56], G. Rabanal Bolanos[61], D. Rafanoharana[54], F. Ragusa[71a,71b], J. L. Rainbolt[39], J. A. Raine[56], S. Rajagopalan[29], E. Ramakoti[37], K. Ran[48,14e], N. P. Rapheeha[33g], H. Rasheed[27b], V. Raskina[127], D. F. Rassloff[63a], S. Rave[100], B. Ravina[55], I. Ravinovich[169], M. Raymond[36], A. L. Read[125], N. P. Readioff[139], D. M. Rebuzzi[73a,73b], G. Redlinger[29], A. S. Reed[110], K. Reeves[26], J. A. Reidelsturz[171,w], D. Reikher[151], A. Rej[141], C. Rembser[36], A. Renardi[48], M. Renda[27b], M. B. Rendel[110], F. Renner[48], A. G. Rennie[59], S. Resconi[71a], M. Ressegotti[57a,57b], S. Rettie[36], J. G. Reyes Rivera[107], B. Reynolds[119], E. Reynolds[17a], O. L. Rezanova[37], P. Reznicek[133], N. Ribaric[91], E. Ricci[78a,78b], R. Richter[110], S. Richter[47a,47b], E. Richter-Was[86b], M. Ridel[127], S. Ridouani[35d], P. Rieck[117], P. Riedler[36], M. Rijssenbeek[145], A. Rimoldi[73a,73b], M. Rimoldi[48], L. Rinaldi[23a,23b], T. T. Rinn[29], M. P. Rinnagel[109], G. Ripellino[161], I. Riu[13], P. Rivadeneira[48], J. C. Rivera Vergara[165], F. Rizatdinova[121], E. Rizvi[94], B. A. Roberts[167], B. R. Roberts[17a], S. H. Robertson[104,ac], M. Robin[48], D. Robinson[32], C. M. Robles Gajardo[137f], M. Robles Manzano[100], A. Robson[59], A. Rocchi[76a,76b], C. Roda[74a,74b], S. Rodriguez Bosca[63a], Y. Rodriguez Garcia[22a], A. Rodriguez Rodriguez[54], A. M. Rodríguez Vera[156b], S. Roe[36], J. T. Roemer[160], A. R. Roepe-Gier[136], J. Roggel[171], O. Røhne[125], R. A. Rojas[103], C. P. A. Roland[68], J. Roloff[29], A. Romaniouk[37], E. Romano[73a,73b], M. Romano[23b], A. C. Romero Hernandez[162], N. Rompotis[92], L. Roos[127], S. Rosati[75a], B. J. Rosser[39], E. Rossi[126], E. Rossi[72a,72b], L. P. Rossi[57b], L. Rossini[48], R. Rosten[119], M. Rotaru[27b], B. Rottler[54], C. Rougier[102,ah], D. Rousseau[66], D. Rousso[32], A. Roy[162], S. Roy-Garand[155], A. Rozanov[102], Y. Rozen[150], X. Ruan[33g], A. Rubio Jimenez[163], A. J. Ruby[92], V. H. Ruelas Rivera[18], T. A. Ruggeri[1], A. Ruggiero[126], A. Ruiz-Martinez[163], A. Rummler[36], Z. Rurikova[54], N. A. Rusakovich[38], H. L. Russell[165], G. Russo[75a,75b], J. P. Rutherfoord[7], S. Rutherford Colmenares[32], K. Rybacki[91], M. Rybar[133], E. B. Rye[125], A. Ryzhov[44], J. A. Sabater Iglesias[56], P. Sabatini[163], L. Sabetta[75a,75b], H. F.-W. Sadrozinski[136], F. Safai Tehrani[75a], B. Safarzadeh Samani[146], M. Safdari[143], S. Saha[165], M. Sahinsoy[110], M. Saimpert[135], M. Saito[153], T. Saito[153], D. Salamani[36], A. Salnikov[143], J. Salt[163], A. Salvador Salas[13], D. Salvatore[43a,43b], F. Salvatore[146], A. Salzburger[36], D. Sammel[54], D. Sampsonidis[152,f], D. Sampsonidou[123], J. Sánchez[163], A. Sanchez Pineda[4], V. Sanchez Sebastian[163], H. Sandaker[125], C. O. Sander[48], J. A. Sandesara[103], M. Sandhoff[171], C. Sandoval[22b], D. P. C. Sankey[134], T. Sano[88], A. Sansoni[53], L. Santi[75a,75b], C. Santoni[40], H. Santos[130a,130b], S. N. Santpur[17a], A. Santra[169], K. A. Saoucha[139], J. G. Saraiva[130a,130d], J. Sardain[7], O. Sasaki[84], K. Sato[157], C. Sauer[63b], F. Sauerburger[54], E. Sauvan[4], P. Savard[155,an], R. Sawada[153], C. Sawyer[134], L. Sawyer[97], I. Sayago Galvan[163], C. Sbarra[23b], A. Sbrizzi[23a,23b], T. Scanlon[96], J. Schaarschmidt[138], P. Schacht[110], D. Schaefer[39], U. Schäfer[100], A. C. Schaffer[66,44], D. Schaile[109], R. D. Schamberger[145], C. Scharf[18], M. M. Schefer[19], V. A. Schegelsky[37], D. Scheirich[133], F. Schenck[18], M. Schernau[160], C. Scheulen[55], C. Schiavi[57a,57b], E. J. Schioppa[70a,70b], M. Schioppa[43a,43b], B. Schlag[143,s], K. E. Schleicher[54], S. Schlenker[36], J. Schmeing[171], M. A. Schmidt[171], K. Schmieden[100], C. Schmitt[100], S. Schmitt[48], L. Schoeffel[135], A. Schoening[63b], P. G. Scholer[54], E. Schopf[126], M. Schott[100], J. Schovancova[36], S. Schramm[56], F. Schroeder[171], T. Schroer[56], H.-C. Schultz-Coulon[63a], M. Schumacher[54], B. A. Schumm[136], Ph. Schune[135], A. J. Schuy[138], H. R. Schwartz[136], A. Schwartzman[143], T. A. Schwarz[106], Ph. Schwemling[135], R. Schwienhorst[107], A. Sciandra[136], G. Sciolla[26], F. Scuri[74a], C. D. Sebastiani[92], K. Sedlaczek[115], P. Seema[18], S. C. Seidel[112], A. Seiden[136], B. D. Seidlitz[41], C. Seitz[48], J. M. Seixas[83b], G. Sekhniaidze[72a], S. J. Sekula[44], L. Selem[60], N. Semprini-Cesari[23a,23b], D. Sengupta[56], V. Senthilkumar[163], L. Serin[66], L. Serkin[69a,69b], M. Sessa[76a,76b], H. Severini[120], F. Sforza[57a,57b], A. Sfyrla[56], E. Shabalina[55], R. Shaheen[144], J. D. Shahinian[128], D. Shaked Renous[169], L. Y. Shan[14a], M. Shapiro[17a], A. Sharma[36], A. S. Sharma[164], P. Sharma[80], S. Sharma[48], P. B. Shatalov[37], K. Shaw[146], S. M. Shaw[101], A. Shcherbakova[37], Q. Shen[5,62c], P. Sherwood[96], L. Shi[96], X. Shi[14a], C. O. Shimmin[172], Y. Shimogama[168], J. D. Shinner[95], I. P. J. Shipsey[126], S. Shirabe[56,i], M. Shiyakova[38,aa],

J. Shlomi[169], M. J. Shochet[39], J. Shojaii[105], D. R. Shope[125], B. Shrestha[120], S. Shrestha[119,aq], E. M. Shrif[33g], M. J. Shroff[165], P. Sicho[131], A. M. Sickles[162], E. Sideras Haddad[33g], A. Sidoti[23b], F. Siegert[50], Dj. Sijacki[15], R. Sikora[86a], F. Sili[90], J. M. Silva[20], M. V. Silva Oliveira[29], S. B. Silverstein[47a], S. Simion[66], R. Simoniello[36], E. L. Simpson[59], H. Simpson[146], L. R. Simpson[106], N. D. Simpson[98], S. Simsek[82], S. Sindhu[55], P. Sinervo[155], S. Singh[155], S. Sinha[48], S. Sinha[101], M. Sioli[23a,23b], I. Siral[36], E. Sitnikova[48], S. Yu. Sivoklokov[37,*], J. Sjölin[47a,47b], A. Skaf[55], E. Skorda[20,ak], P. Skubic[120], M. Slawinska[87], V. Smakhtin[169], B. H. Smart[134], J. Smiesko[36], S. Yu. Smirnov[37], Y. Smirnov[37], L. N. Smirnova[37,a], O. Smirnova[98], A. C. Smith[41], E. A. Smith[39], H. A. Smith[126], J. L. Smith[92], R. Smith[143], M. Smizanska[91], K. Smolek[132], A. A. Snesarev[37], S. R. Snider[155], H. L. Snoek[114], S. Snyder[29], R. Sobie[165,ac], A. Soffer[151], C. A. Solans Sanchez[36], E. Yu. Soldatov[37], U. Soldevila[163], A. A. Solodkov[37], S. Solomon[26], A. Soloshenko[38], K. Solovieva[54], O. V. Solovyanov[40], V. Solovyev[37], P. Sommer[36], A. Sonay[13], W. Y. Song[156b], J. M. Sonneveld[114], A. Sopczak[132], A. L. Sopio[96], F. Sopkova[28b], V. Sothilingam[63a], S. Sottocornola[68], R. Soualah[116b], Z. Soumaimi[35e], D. South[48], S. Spagnolo[70a,70b], M. Spalla[110], D. Sperlich[54], G. Spigo[36], M. Spina[146], S. Spinali[91], D. P. Spiteri[59], M. Spousta[133], E. J. Staats[34], A. Stabile[71a,71b], R. Stamen[63a], M. Stamenkovic[114], A. Stampekis[20], M. Standke[24], E. Stanecka[87], M. V. Stange[50], B. Stanislaus[17a], M. M. Stanitzki[48], B. Stapf[48], E. A. Starchenko[37], G. H. Stark[136], J. Stark[102,ah], D. M. Starko[156b], P. Staroba[131], P. Starovoitov[63a], S. Stärz[104], R. Staszewski[87], G. Stavropoulos[46], J. Steentoft[161], P. Steinberg[29], B. Stelzer[142,156a], H. J. Stelzer[129], O. Stelzer-Chilton[156a], H. Stenzel[58], T. J. Stevenson[146], G. A. Stewart[36], J. R. Stewart[121], M. C. Stockton[36], G. Stoicea[27b], M. Stolarski[130a], S. Stonjek[110], A. Straessner[50], J. Strandberg[144], S. Strandberg[47a,47b], M. Strauss[120], T. Strebler[102], P. Strizenec[28b], R. Ströhmer[166], D. M. Strom[123], L. R. Strom[48], R. Stroynowski[44], A. Strubig[47a,47b], S. A. Stucci[29], B. Stugu[16], J. Stupak[120], N. A. Styles[48], D. Su[143], S. Su[62a], W. Su[62d], X. Su[62a,66], K. Sugizaki[153], V. V. Sulin[37], M. J. Sullivan[92], D. M. S. Sultan[78a,78b], L. Sultanaliyeva[37], S. Sultansoy[3b], T. Sumida[88], S. Sun[106], S. Sun[170], O. Sunneborn Gudnadottir[161], N. Sur[102], M. R. Sutton[146], H. Suzuki[157], M. Svatos[131], M. Swiatlowski[156a], T. Swirski[166], I. Sykora[28a], M. Sykora[133], T. Sykora[133], D. Ta[100], K. Tackmann[48,z], A. Taffard[160], R. Tafirout[156a], J. S. Tafoya Vargas[66], E. P. Takeva[52], Y. Takubo[84], M. Talby[102], A. A. Talyshev[37], K. C. Tam[64b], N. M. Tamir[151], A. Tanaka[153], J. Tanaka[153], R. Tanaka[66], M. Tanasini[57a,57b], Z. Tao[164], S. Tapia Araya[137f], S. Tapprogge[100], A. Tarek Abouelfadl Mohamed[107], S. Tarem[150], K. Tariq[14a], G. Tarna[27b,102], G. F. Tartarelli[71a], P. Tas[133], M. Tasevsky[131], E. Tassi[43a,43b], A. C. Tate[162], G. Tateno[153], Y. Tayalati[35e,ab], G. N. Taylor[105], W. Taylor[156b], H. Teagle[92], A. S. Tee[170], R. Teixeira De Lima[143], P. Teixeira-Dias[95], J. J. Teoh[155], K. Terashi[153], J. Terron[99], S. Terzo[13], M. Testa[53], R. J. Teuscher[155,ac], A. Thaler[79], O. Theiner[56], N. Themistokleous[52], T. Theveneaux-Pelzer[102], O. Thielmann[171], D. W. Thomas[95], J. P. Thomas[20], E. A. Thompson[17a], P. D. Thompson[20], E. Thomson[128], Y. Tian[55], V. Tikhomirov[37,a], Yu. A. Tikhonov[37], S. Timoshenko[37], D. Timoshyn[133], E. X. L. Ting[1], P. Tipton[172], S. H. Tlou[33g], A. Tnourji[40], K. Todome[23a,23b], S. Todorova-Nova[133], S. Todt[50], M. Togawa[84], J. Tojo[89], S. Tokár[28a], K. Tokushuku[84], O. Toldaiev[68], R. Tombs[32], M. Tomoto[84,111], L. Tompkins[143,s], K. W. Topolnicki[86b], E. Torrence[123], H. Torres[102,ah], E. Torró Pastor[163], M. Toscani[30], C. Tosciri[39], M. Tost[11], D. R. Tovey[139], A. Traeet[16], I. S. Trandafir[27b], T. Trefzger[166], A. Tricoli[29], I. M. Trigger[156a], S. Trincaz-Duvoid[127], D. A. Trischuk[26], B. Trocmé[60], C. Troncon[71a], L. Truong[33c], M. Trzebinski[87], A. Trzupek[87], F. Tsai[145], M. Tsai[106], A. Tsiamis[152,f], P. V. Tsiareshka[37], S. Tsigaridas[156a], A. Tsirigotis[152,x], V. Tsiskaridze[155], E. G. Tskhadadze[149a], M. Tsopoulou[152,f], Y. Tsujikawa[88], I. I. Tsukerman[37], V. Tsulaia[17a], S. Tsuno[84], O. Tsur[150], K. Tsuri[118], D. Tsybychev[145], Y. Tu[64b], A. Tudorache[27b], V. Tudorache[27b], A. N. Tuna[36], S. Turchikhin[38], I. Turk Cakir[3a], R. Turra[71a], T. Turtuvshin[38,ad], P. M. Tuts[41], S. Tzamarias[152,f], P. Tzanis[10], E. Tzovara[100], K. Uchida[153], F. Ukegawa[157], P. A. Ulloa Poblete[137b,137c], E. N. Umaka[29], G. Unal[36], M. Unal[11], A. Undrus[29], G. Unel[160], J. Urban[28b], P. Urquijo[105], G. Usai[8], R. Ushioda[154], M. Usman[108], Z. Uysal[21b], L. Vacavant[102], V. Vacek[132], B. Vachon[104], K. O. H. Vadla[125], T. Vafeiadis[36], A. Vaitkus[96], C. Valderanis[109], E. Valdes Santurio[47a,47b], M. Valente[156a], S. Valentinetti[23a,23b], A. Valero[163], E. Valiente Moreno[163], A. Vallier[102,ah], J. A. Valls Ferrer[163], D. R. Van Arneman[114], T. R. Van Daalen[138], A. Van Der Graaf[49], P. Van Gemmeren[6], M. Van Rijnbach[36,125], S. Van Stroud[96], I. Van Vulpen[114], M. Vanadia[76a,76b], W. Vandelli[36], M. Vandenbroucke[135], E. R. Vandewall[121], D. Vannicola[151], L. Vannoli[57a,57b], R. Vari[75a], E. W. Varnes[7], C. Varni[17b], T. Varol[148], D. Varouchas[66], L. Varriale[163], K. E. Varvell[147], M. E. Vasile[27b], L. Vaslin[40], G. A. Vasquez[165], F. Vazeille[40], T. Vazquez Schroeder[36], J. Veatch[31], V. Vecchio[101], M. J. Veen[103], I. Veliscek[126], L. M. Veloce[155],

F. Veloso[130a,130c], S. Veneziano[75a], A. Ventura[70a,70b], A. Verbytskyi[110], M. Verducci[74a,74b], C. Vergis[24], M. Verissimo De Araujo[83b], W. Verkerke[114], J. C. Vermeulen[114], C. Vernieri[143], M. Vessella[103], M. C. Vetterli[142,an], A. Vgenopoulos[152,f], N. Viaux Maira[137f], T. Vickey[139], O. E. Vickey Boeriu[139], G. H. A. Viehhauser[126], L. Vigani[63b], M. Villa[23a,23b], M. Villaplana Perez[163], E. M. Villhauer[52], E. Vilucchi[53], M. G. Vincter[34], G. S. Virdee[20], A. Vishwakarma[52], A. Visibile[114], C. Vittori[36], I. Vivarelli[146], V. Vladimirov[167], E. Voevodina[110], F. Vogel[109], P. Vokac[132], J. Von Ahnen[48], E. Von Toerne[24], B. Vormwald[36], V. Vorobel[133], K. Vorobev[37], M. Vos[163], K. Voss[141], J. H. Vossebeld[92], M. Vozak[114], L. Vozdecky[94], N. Vranjes[15], M. Vranjes Milosavljevic[15], M. Vreeswijk[114], N. K. Vu[62c,62d], R. Vuillermet[36], O. Vujinovic[100], I. Vukotic[39], S. Wada[157], C. Wagner[103], J. M. Wagner[17a], W. Wagner[171], S. Wahdan[171], H. Wahlberg[90], R. Wakasa[157], M. Wakida[111], J. Walder[134], R. Walker[109], W. Walkowiak[141], A. Wall[128], T. Wamorkar[6], A. Z. Wang[170], C. Wang[100], C. Wang[62c], H. Wang[17a], J. Wang[64a], R. -J. Wang[100], R. Wang[61], R. Wang[6], S. M. Wang[148], S. Wang[62b], T. Wang[62a], W. T. Wang[80], W. Wang[14a], X. Wang[14c], X. Wang[162], X. Wang[62c], Y. Wang[62d], Y. Wang[14c], Z. Wang[106], Z. Wang[51,62c,62d], Z. Wang[106], A. Warburton[104], R. J. Ward[20], N. Warrack[59], A. T. Watson[20], H. Watson[59], M. F. Watson[20], E. Watton[59,134], G. Watts[138], B. M. Waugh[96], C. Weber[29], H. A. Weber[18], M. S. Weber[19], S. M. Weber[63a], C. Wei[62a], Y. Wei[126], A. R. Weidberg[126], E. J. Weik[117], J. Weingarten[49], M. Weirich[100], C. Weiser[54], C. J. Wells[48], T. Wenaus[29], B. Wendland[49], T. Wengler[36], N. S. Wenke[110], N. Wermes[24], M. Wessels[63a], K. Whalen[123], A. M. Wharton[91], A. S. White[61], A. White[8], M. J. White[1], D. Whiteson[160], L. Wickremasinghe[124], W. Wiedenmann[170], C. Wiel[50], M. Wielers[134], C. Wiglesworth[42], D. J. Wilbern[120], H. G. Wilkens[36], D. M. Williams[41], H. H. Williams[128], S. Williams[32], S. Willocq[103], B. J. Wilson[101], P. J. Windischhofer[39], F. I. Winkel[30], F. Winklmeier[123], B. T. Winter[54], J. K. Winter[101], M. Wittgen[143], M. Wobisch[97], Z. Wolffs[114], R. Wölker[126], J. Wollrath[160], M. W. Wolter[87], H. Wolters[130a,130c], A. F. Wongel[48], S. D. Worm[48], B. K. Wosiek[87], K. W. Woźniak[87], S. Wozniewski[55], K. Wraight[59], C. Wu[20], J. Wu[14a,14e], M. Wu[64a], M. Wu[113], S. L. Wu[170], X. Wu[56], Y. Wu[62a], Z. Wu[135], J. Wuerzinger[110,al], T. R. Wyatt[101], B. M. Wynne[52], S. Xella[42], L. Xia[14c], M. Xia[14b], J. Xiang[64c], X. Xiao[106], M. Xie[62a], X. Xie[62a], S. Xin[14a,14e], J. Xiong[17a], D. Xu[14a], H. Xu[62a], L. Xu[62a], R. Xu[128], T. Xu[106], Y. Xu[14b], Z. Xu[52], Z. Xu[14a], B. Yabsley[147], S. Yacoob[33a], N. Yamaguchi[89], Y. Yamaguchi[154], E. Yamashita[153], H. Yamauchi[157], T. Yamazaki[17a], Y. Yamazaki[85], J. Yan[62c], S. Yan[126], Z. Yan[25], H. J. Yang[62c,62d], H. T. Yang[62a], S. Yang[62a], T. Yang[64c], X. Yang[62a], X. Yang[14a], Y. Yang[44], Y. Yang[62a], Z. Yang[62a], W.-M. Yao[17a], Y. C. Yap[48], H. Ye[14c], H. Ye[55], J. Ye[44], S. Ye[29], X. Ye[62a], Y. Yeh[96], I. Yeletskikh[38], B. K. Yeo[17b], M. R. Yexley[96], P. Yin[41], K. Yorita[168], S. Younas[27b], C. J. S. Young[36], C. Young[143], Y. Yu[62a], M. Yuan[106], R. Yuan[62b,l], L. Yue[96], M. Zaazoua[62a], B. Zabinski[87], E. Zaid[52], T. Zakareishvili[149b], N. Zakharchuk[34], S. Zambito[56], J. A. Zamora Saa[137b,137d], J. Zang[153], D. Zanzi[54], O. Zaplatilek[132], C. Zeitnitz[171], H. Zeng[14a], J. C. Zeng[162], D. T. Zenger Jr[26], O. Zenin[37], T. Ženiš[28a], S. Zenz[94], S. Zerradi[35a], D. Zerwas[66], M. Zhai[14a,14e], B. Zhang[14c], D. F. Zhang[139], J. Zhang[62b], J. Zhang[6], K. Zhang[14a,14e], L. Zhang[14c], P. Zhang[14a,14e], R. Zhang[170], S. Zhang[106], T. Zhang[153], X. Zhang[62c], X. Zhang[62b], Y. Zhang[5,62c], Y. Zhang[96], Z. Zhang[17a], Z. Zhang[66], H. Zhao[138], P. Zhao[51], T. Zhao[62b], Y. Zhao[136], Z. Zhao[62a], A. Zhemchugov[38], K. Zheng[162], X. Zheng[62a], Z. Zheng[143], D. Zhong[162], B. Zhou[106], H. Zhou[7], N. Zhou[62c], Y. Zhou[7], C. G. Zhu[62b], J. Zhu[106], Y. Zhu[62c], Y. Zhu[62a], X. Zhuang[14a], K. Zhukov[37], V. Zhulanov[37], N. I. Zimine[38], J. Zinsser[63b], M. Ziolkowski[141], L. Živković[15], A. Zoccoli[23a,23b], K. Zoch[56], T. G. Zorbas[139], O. Zormpa[46], W. Zou[41], L. Zwalinski[36]

[1] Department of Physics, University of Adelaide, Adelaide, Australia
[2] Department of Physics, University of Alberta, Edmonton, AB, Canada
[3] [(a)]Department of Physics, Ankara University, Ankara, Türkiye; [(b)]Division of Physics, TOBB University of Economics and Technology, Ankara, Türkiye
[4] LAPP, Université Savoie Mont Blanc, CNRS/IN2P3, Annecy, France
[5] APC, Université Paris Cité, CNRS/IN2P3, Paris, France
[6] High Energy Physics Division, Argonne National Laboratory, Argonne, IL, USA
[7] Department of Physics, University of Arizona, Tucson, AZ, USA
[8] Department of Physics, University of Texas at Arlington, Arlington, TX, USA
[9] Physics Department, National and Kapodistrian University of Athens, Athens, Greece
[10] Physics Department, National Technical University of Athens, Zografou, Greece
[11] Department of Physics, University of Texas at Austin, Austin, TX, USA

[12] Institute of Physics, Azerbaijan Academy of Sciences, Baku, Azerbaijan
[13] Institut de Física d'Altes Energies (IFAE), Barcelona Institute of Science and Technology, Barcelona, Spain
[14] [(a)]Institute of High Energy Physics, Chinese Academy of Sciences, Beijing, China; [(b)]Physics Department, Tsinghua University, Beijing, China; [(c)]Department of Physics, Nanjing University, Nanjing, China; [(d)]School of Science, Shenzhen Campus of Sun Yat-sen University, Guangzhou, China; [(e)]University of Chinese Academy of Science (UCAS), Beijing, China
[15] Institute of Physics, University of Belgrade, Belgrade, Serbia
[16] Department for Physics and Technology, University of Bergen, Bergen, Norway
[17] [(a)]Physics Division, Lawrence Berkeley National Laboratory, Berkeley, CA, USA; [(b)]University of California, Berkeley, CA, USA
[18] Institut für Physik, Humboldt Universität zu Berlin, Berlin, Germany
[19] Albert Einstein Center for Fundamental Physics and Laboratory for High Energy Physics, University of Bern, Bern, Switzerland
[20] School of Physics and Astronomy, University of Birmingham, Birmingham, UK
[21] [(a)]Department of Physics, Bogazici University, Istanbul, Türkiye; [(b)]Department of Physics Engineering, Gaziantep University, Gaziantep, Türkiye; [(c)]Department of Physics, Istanbul University, Istanbul, Türkiye
[22] [(a)]Facultad de Ciencias y Centro de Investigaciónes, Universidad Antonio Nariño, Bogotá, Colombia; [(b)]Departamento de Física, Universidad Nacional de Colombia, Bogotá, Colombia
[23] [(a)]Dipartimento di Fisica e Astronomia A. Righi, Università di Bologna, Bologna, Italy; [(b)]INFN Sezione di Bologna, Bologna, Italy
[24] Physikalisches Institut, Universität Bonn, Bonn, Germany
[25] Department of Physics, Boston University, Boston, MA, USA
[26] Department of Physics, Brandeis University, Waltham, MA, USA
[27] [(a)]Transilvania University of Brasov, Brasov, Romania; [(b)]Horia Hulubei National Institute of Physics and Nuclear Engineering, Bucharest, Romania; [(c)]Department of Physics, Alexandru Ioan Cuza University of Iasi, Iasi, Romania; [(d)]Physics Department, National Institute for Research and Development of Isotopic and Molecular Technologies, Cluj-Napoca, Romania; [(e)]University Politehnica Bucharest, Bucharest, Romania; [(f)]West University in Timisoara, Timisoara, Romania; [(g)]Faculty of Physics, University of Bucharest, Bucharest, Romania
[28] [(a)]Faculty of Mathematics, Physics and Informatics, Comenius University, Bratislava, Slovak Republic; [(b)]Department of Subnuclear Physics, Institute of Experimental Physics of the Slovak Academy of Sciences, Kosice, Slovak Republic
[29] Physics Department, Brookhaven National Laboratory, Upton, NY, USA
[30] Universidad de Buenos Aires, Facultad de Ciencias Exactas y Naturales, Departamento de Física, y CONICET, Instituto de Física de Buenos Aires (IFIBA), Buenos Aires, Argentina
[31] California State University, Los Angeles, CA, USA
[32] Cavendish Laboratory, University of Cambridge, Cambridge, UK
[33] [(a)]Department of Physics, University of Cape Town, Cape Town, South Africa; [(b)]iThemba Labs, Western Cape, South Africa; [(c)]Department of Mechanical Engineering Science, University of Johannesburg, Johannesburg, South Africa ; [(d)]National Institute of Physics, University of the Philippines, Diliman, Philippines; [(e)]Department of Physics, University of South Africa, Pretoria, South Africa; [(f)]University of Zululand, KwaDlangezwa, South Africa; [(g)]School of Physics, University of the Witwatersrand, Johannesburg, South Africa
[34] Department of Physics, Carleton University, Ottawa, ON, Canada
[35] [(a)]Faculté des Sciences Ain Chock, Réseau Universitaire de Physique des Hautes Energies-Université Hassan II, Casablanca, Morocco; [(b)]Faculté des Sciences, Université Ibn-Tofail, Kénitra, Morocco; [(c)]Faculté des Sciences Semlalia, Université Cadi Ayyad, LPHEA-Marrakech, Morocco; [(d)]LPMR, Faculté des Sciences, Université Mohamed Premier, Oujda, Morocco; [(e)]Faculté des sciences, Université Mohammed V, Rabat, Morocco; [(f)]Institute of Applied Physics, Mohammed VI Polytechnic University, Ben Guerir, Morocco
[36] CERN, Geneva, Switzerland
[37] Affiliated with an institute covered by a cooperation agreement with CERN, Geneva, Switzerland
[38] Affiliated with an international laboratory covered by a cooperation agreement with CERN, Geneva, Switzerland
[39] Enrico Fermi Institute, University of Chicago, Chicago, IL, USA
[40] LPC, Université Clermont Auvergne, CNRS/IN2P3, Clermont-Ferrand, France
[41] Nevis Laboratory, Columbia University, Irvington, NY, USA
[42] Niels Bohr Institute, University of Copenhagen, Copenhagen, Denmark

[43] [(a)]Dipartimento di Fisica, Università della Calabria, Rende, Italy; [(b)]INFN Gruppo Collegato di Cosenza, Laboratori Nazionali di Frascati, Frascati, Italy
[44] Physics Department, Southern Methodist University, Dallas, TX, USA
[45] Physics Department, University of Texas at Dallas, Richardson, TX, USA
[46] National Centre for Scientific Research "Demokritos", Agia Paraskevi, Greece
[47] [(a)]Department of Physics, Stockholm University, Stockholm, Sweden; [(b)]Oskar Klein Centre, Stockholm, Sweden
[48] Deutsches Elektronen-Synchrotron DESY, Hamburg and Zeuthen, Germany
[49] Fakultät Physik , Technische Universität Dortmund, Dortmund, Germany
[50] Institut für Kern- und Teilchenphysik, Technische Universität Dresden, Dresden, Germany
[51] Department of Physics, Duke University, Durham, NC, USA
[52] SUPA-School of Physics and Astronomy, University of Edinburgh, Edinburgh, UK
[53] INFN e Laboratori Nazionali di Frascati, Frascati, Italy
[54] Physikalisches Institut, Albert-Ludwigs-Universität Freiburg, Freiburg, Germany
[55] II. Physikalisches Institut, Georg-August-Universität Göttingen, Göttingen, Germany
[56] Département de Physique Nucléaire et Corpusculaire, Université de Genève, Geneva, Switzerland
[57] [(a)]Dipartimento di Fisica, Università di Genova, Genoa, Italy; [(b)]INFN Sezione di Genova, Genoa, Italy
[58] II. Physikalisches Institut, Justus-Liebig-Universität Giessen, Giessen, Germany
[59] SUPA-School of Physics and Astronomy, University of Glasgow, Glasgow, UK
[60] LPSC, Université Grenoble Alpes, CNRS/IN2P3, Grenoble INP, Grenoble, France
[61] Laboratory for Particle Physics and Cosmology, Harvard University, Cambridge, MA, USA
[62] [(a)]Department of Modern Physics and State Key Laboratory of Particle Detection and Electronics, University of Science and Technology of China, Hefei, China; [(b)]Institute of Frontier and Interdisciplinary Science and Key Laboratory of Particle Physics and Particle Irradiation (MOE), Shandong University, Qingdao, China; [(c)]School of Physics and Astronomy, Shanghai Jiao Tong University, Key Laboratory for Particle Astrophysics and Cosmology (MOE), SKLPPC, Shanghai, China; [(d)]Tsung-Dao Lee Institute, Shanghai, China
[63] [(a)]Kirchhoff-Institut für Physik, Ruprecht-Karls-Universität Heidelberg, Heidelberg, Germany; [(b)]Physikalisches Institut, Ruprecht-Karls-Universität Heidelberg, Heidelberg, Germany
[64] [(a)]Department of Physics, Chinese University of Hong Kong, Shatin N.T., Hong Kong, China; [(b)]Department of Physics, University of Hong Kong, Hong Kong, China; [(c)]Department of Physics and Institute for Advanced Study, Hong Kong University of Science and Technology, Clear Water Bay, Kowloon, Hong Kong, China
[65] Department of Physics, National Tsing Hua University, Hsinchu, Taiwan
[66] IJCLab, Université Paris-Saclay, CNRS/IN2P3, 91405 Orsay, France
[67] Centro Nacional de Microelectrónica (IMB-CNM-CSIC), Barcelona, Spain
[68] Department of Physics, Indiana University, Bloomington, IN, USA
[69] [(a)]INFN Gruppo Collegato di Udine, Sezione di Trieste, Udine, Italy; [(b)]ICTP, Trieste, Italy; [(c)]Dipartimento Politecnico di Ingegneria e Architettura, Università di Udine, Udine, Italy
[70] [(a)]INFN Sezione di Lecce, Lecce, Italy; [(b)]Dipartimento di Matematica e Fisica, Università del Salento, Lecce, Italy
[71] [(a)]INFN Sezione di Milano, Milan, Italy; [(b)]Dipartimento di Fisica, Università di Milano, Milan, Italy
[72] [(a)]INFN Sezione di Napoli, Naples, Italy; [(b)]Dipartimento di Fisica, Università di Napoli, Naples, Italy
[73] [(a)]INFN Sezione di Pavia, Pavia, Italy; [(b)]Dipartimento di Fisica, Università di Pavia, Pavia, Italy
[74] [(a)]INFN Sezione di Pisa, Pisa, Italy; [(b)]Dipartimento di Fisica E. Fermi, Università di Pisa, Pisa, Italy
[75] [(a)]INFN Sezione di Roma, Rome, Italy; [(b)]Dipartimento di Fisica, Sapienza Università di Roma, Rome, Italy
[76] [(a)]INFN Sezione di Roma Tor Vergata, Rome, Italy; [(b)]Dipartimento di Fisica, Università di Roma Tor Vergata, Rome, Italy
[77] [(a)]INFN Sezione di Roma Tre, Rome, Italy; [(b)]Dipartimento di Matematica e Fisica, Università Roma Tre, Rome, Italy
[78] [(a)]INFN-TIFPA, Povo, Italy; [(b)]Università degli Studi di Trento, Trento, Italy
[79] Universität Innsbruck, Department of Astro and Particle Physics, Innsbruck, Austria
[80] University of Iowa, Iowa City, IA, USA
[81] Department of Physics and Astronomy, Iowa State University, Ames, IA, USA
[82] Istinye University, Sariyer, Istanbul, Türkiye
[83] [(a)]Departamento de Engenharia Elétrica, Universidade Federal de Juiz de Fora (UFJF), Juiz de Fora, Brazil; [(b)]Universidade Federal do Rio De Janeiro COPPE/EE/IF, Rio de Janeiro, Brazil; [(c)]Instituto de Física, Universidade de São Paulo, São Paulo, Brazil; [(d)]Rio de Janeiro State University, Rio de Janeiro, Brazil

[84] KEK, High Energy Accelerator Research Organization, Tsukuba, Japan
[85] Graduate School of Science, Kobe University, Kobe, Japan
[86] [(a)]AGH University of Krakow, Faculty of Physics and Applied Computer Science, Kraków, Poland; [(b)]Marian Smoluchowski Institute of Physics, Jagiellonian University, Kraków, Poland
[87] Institute of Nuclear Physics Polish Academy of Sciences, Kraków, Poland
[88] Faculty of Science, Kyoto University, Kyoto, Japan
[89] Research Center for Advanced Particle Physics and Department of Physics, Kyushu University, Fukuoka , Japan
[90] Instituto de Física La Plata, Universidad Nacional de La Plata and CONICET, La Plata, Argentina
[91] Physics Department, Lancaster University, Lancaster, UK
[92] Oliver Lodge Laboratory, University of Liverpool, Liverpool, UK
[93] Department of Experimental Particle Physics, Jožef Stefan Institute and Department of Physics, University of Ljubljana, Ljubljana, Slovenia
[94] School of Physics and Astronomy, Queen Mary University of London, London, UK
[95] Department of Physics, Royal Holloway University of London, Egham, UK
[96] Department of Physics and Astronomy, University College London, London, UK
[97] Louisiana Tech University, Ruston, LA, USA
[98] Fysiska institutionen, Lunds universitet, Lund, Sweden
[99] Departamento de Física Teorica C-15 and CIAFF, Universidad Autónoma de Madrid, Madrid, Spain
[100] Institut für Physik, Universität Mainz, Mainz, Germany
[101] School of Physics and Astronomy, University of Manchester, Manchester, UK
[102] CPPM, Aix-Marseille Université, CNRS/IN2P3, Marseille, France
[103] Department of Physics, University of Massachusetts, Amherst, MA, USA
[104] Department of Physics, McGill University, Montreal, QC, Canada
[105] School of Physics, University of Melbourne, Melbourne, VIC, Australia
[106] Department of Physics, University of Michigan, Ann Arbor, MI, USA
[107] Department of Physics and Astronomy, Michigan State University, East Lansing, MI, USA
[108] Group of Particle Physics, University of Montreal, Montreal, QC, Canada
[109] Fakultät für Physik, Ludwig-Maximilians-Universität München, Munich, Germany
[110] Max-Planck-Institut für Physik (Werner-Heisenberg-Institut), Munich, Germany
[111] Graduate School of Science and Kobayashi-Maskawa Institute, Nagoya University, Nagoya, Japan
[112] Department of Physics and Astronomy, University of New Mexico, Albuquerque, NM, USA
[113] Institute for Mathematics, Astrophysics and Particle Physics, Radboud University/Nikhef, Nijmegen, The Netherlands
[114] Nikhef National Institute for Subatomic Physics and University of Amsterdam, Amsterdam, The Netherlands
[115] Department of Physics, Northern Illinois University, DeKalb, IL, USA
[116] [(a)]New York University Abu Dhabi, Abu Dhabi, United Arab Emirates; [(b)]University of Sharjah, Sharjah, United Arab Emirates
[117] Department of Physics, New York University, New York, NY, USA
[118] Ochanomizu University, Otsuka, Bunkyo-ku, Tokyo, Japan
[119] Ohio State University, Columbus, OH, USA
[120] Homer L. Dodge Department of Physics and Astronomy, University of Oklahoma, Norman, OK, USA
[121] Department of Physics, Oklahoma State University, Stillwater, OK, USA
[122] Palacký University, Joint Laboratory of Optics, Olomouc, Czech Republic
[123] Institute for Fundamental Science, University of Oregon, Eugene, OR, USA
[124] Graduate School of Science, Osaka University, Osaka, Japan
[125] Department of Physics, University of Oslo, Oslo, Norway
[126] Department of Physics, Oxford University, Oxford, UK
[127] LPNHE, Sorbonne Université, Université Paris Cité, CNRS/IN2P3, Paris, France
[128] Department of Physics, University of Pennsylvania, Philadelphia, PA, USA
[129] Department of Physics and Astronomy, University of Pittsburgh, Pittsburgh, PA, USA
[130] [(a)]Laboratório de Instrumentação e Física Experimental de Partículas - LIP, Lisbon, Portugal; [(b)]Departamento de Física, Faculdade de Ciências, Universidade de Lisboa, Lisbon, Portugal; [(c)]Departamento de Física, Universidade de Coimbra, Coimbra, Portugal; [(d)]Centro de Física Nuclear da Universidade de Lisboa, Lisbon, Portugal; [(e)]Departamento de Física,

Universidade do Minho, Braga, Portugal; [f]Departamento de Física Teórica y del Cosmos, Universidad de Granada, Granada, Spain; [g]Departamento de Física, Instituto Superior Técnico, Universidade de Lisboa, Lisbon, Portugal
[131] Institute of Physics of the Czech Academy of Sciences, Prague, Czech Republic
[132] Czech Technical University in Prague, Prague, Czech Republic
[133] Faculty of Mathematics and Physics, Charles University, Prague, Czech Republic
[134] Particle Physics Department, Rutherford Appleton Laboratory, Didcot, UK
[135] IRFU, CEA, Université Paris-Saclay, Gif-sur-Yvette, France
[136] Santa Cruz Institute for Particle Physics, University of California Santa Cruz, Santa Cruz, CA, USA
[137] [a]Departamento de Física, Pontificia Universidad Católica de Chile, Santiago, Chile; [b]Millennium Institute for Subatomic physics at high energy frontier (SAPHIR), Santiago, Chile; [c]Instituto de Investigación Multidisciplinario en Ciencia y Tecnología y Departamento de Física, Universidad de La Serena, La Serena, Chile; [d]Universidad Andres Bello, Department of Physics, Santiago, Chile; [e]Instituto de Alta Investigación, Universidad de Tarapacá, Arica, Chile ; [f]Departamento de Física, Universidad Técnica Federico Santa María, Valparaíso, Chile
[138] Department of Physics, University of Washington, Seattle, WA, USA
[139] Department of Physics and Astronomy, University of Sheffield, Sheffield, UK
[140] Department of Physics, Shinshu University, Nagano, Japan
[141] Department Physik, Universität Siegen, Siegen, Germany
[142] Department of Physics, Simon Fraser University, Burnaby, BC, Canada
[143] SLAC National Accelerator Laboratory, Stanford, CA, USA
[144] Department of Physics, Royal Institute of Technology, Stockholm, Sweden
[145] Departments of Physics and Astronomy, Stony Brook University, Stony Brook, NY, USA
[146] Department of Physics and Astronomy, University of Sussex, Brighton, UK
[147] School of Physics, University of Sydney, Sydney, Australia
[148] Institute of Physics, Academia Sinica, Taipei, Taiwan
[149] [a]E. Andronikashvili Institute of Physics, Iv. Javakhishvili Tbilisi State University, Tbilisi, Georgia; [b]High Energy Physics Institute, Tbilisi State University, Tbilisi, Georgia; [c]University of Georgia, Tbilisi, Georgia
[150] Department of Physics, Technion, Israel Institute of Technology, Haifa, Israel
[151] Raymond and Beverly Sackler School of Physics and Astronomy, Tel Aviv University, Tel Aviv, Israel
[152] Department of Physics, Aristotle University of Thessaloniki, Thessaloniki, Greece
[153] International Center for Elementary Particle Physics and Department of Physics, University of Tokyo, Tokyo, Japan
[154] Department of Physics, Tokyo Institute of Technology, Tokyo, Japan
[155] Department of Physics, University of Toronto, Toronto, ON, Canada
[156] [a]TRIUMF, Vancouver, BC, Canada; [b]Department of Physics and Astronomy, York University, Toronto, ON, Canada
[157] Division of Physics and Tomonaga Center for the History of the Universe, Faculty of Pure and Applied Sciences, University of Tsukuba, Tsukuba, Japan
[158] Department of Physics and Astronomy, Tufts University, Medford, MA, USA
[159] United Arab Emirates University, Al Ain, United Arab Emirates
[160] Department of Physics and Astronomy, University of California Irvine, Irvine, CA, USA
[161] Department of Physics and Astronomy, University of Uppsala, Uppsala, Sweden
[162] Department of Physics, University of Illinois, Urbana, IL, USA
[163] Instituto de Física Corpuscular (IFIC), Centro Mixto Universidad de Valencia - CSIC, Valencia, Spain
[164] Department of Physics, University of British Columbia, Vancouver, BC, Canada
[165] Department of Physics and Astronomy, University of Victoria, Victoria, BC, Canada
[166] Fakultät für Physik und Astronomie, Julius-Maximilians-Universität Würzburg, Würzburg, Germany
[167] Department of Physics, University of Warwick, Coventry, UK
[168] Waseda University, Tokyo, Japan
[169] Department of Particle Physics and Astrophysics, Weizmann Institute of Science, Rehovot, Israel
[170] Department of Physics, University of Wisconsin, Madison, WI, USA
[171] Fakultät für Mathematik und Naturwissenschaften, Fachgruppe Physik, Bergische Universität Wuppertal, Wuppertal, Germany
[172] Department of Physics, Yale University, New Haven, CT, USA

[a] Also Affiliated with an institute covered by a cooperation agreement with CERN, Geneva, Switzerland

[b] Also at An-Najah National University, Nablus, Palestine
[c] Also at APC, Université Paris Cité, CNRS/IN2P3, Paris, France
[d] Also at Borough of Manhattan Community College, City University of New York, New York, NY, USA
[e] Also at Center for High Energy Physics, Peking University, Beijing, China
[f] Also at Center for Interdisciplinary Research and Innovation (CIRI-AUTH), Thessaloniki , Greece
[g] Also at Centro Studi e Ricerche Enrico Fermi, Rome, Italy
[h] Also at CERN, Geneva, Switzerland
[i] Also at Département de Physique Nucléaire et Corpusculaire, Université de Genève, Geneva, Switzerland
[j] Also at Departament de Fisica de la Universitat Autonoma de Barcelona, Barcelona, Spain
[k] Also at Department of Financial and Management Engineering, University of the Aegean, Chios, Greece
[l] Also at Department of Physics and Astronomy, Michigan State University, East Lansing, MI, USA
[m] Also at Department of Physics and Astronomy, University of Sheffield, Sheffield, UK
[n] Also at Department of Physics and Astronomy, University of Victoria, Victoria, BC, Canada
[o] Also at Department of Physics, Ben Gurion University of the Negev, Beer Sheva, Israel
[p] Also at Department of Physics, California State University, Sacramento, USA
[q] Also at Department of Physics, King's College London, London, UK
[r] Also at Department of Physics, Royal Holloway University of London, Egham, UK
[s] Also at Department of Physics, Stanford University, Stanford, CA, USA
[t] Also at Department of Physics, University of Fribourg, Fribourg, Switzerland
[u] Also at Department of Physics, University of Thessaly, Thessaly, Greece
[v] Also at Department of Physics, Westmont College, Santa Barbara, USA
[w] Also at Fakultät für Mathematik und Naturwissenschaften, Fachgruppe Physik, Bergische Universität Wuppertal, Wuppertal, Germany
[x] Also at Hellenic Open University, Patras, Greece
[y] Also at Institucio Catalana de Recerca i Estudis Avancats, ICREA, Barcelona, Spain
[z] Also at Institut für Experimentalphysik, Universität Hamburg, Hamburg, Germany
[aa] Also at Institute for Nuclear Research and Nuclear Energy (INRNE) of the Bulgarian Academy of Sciences, Sofia, Bulgaria
[ab] Also at Institute of Applied Physics, Mohammed VI Polytechnic University, Ben Guerir, Morocco
[ac] Also at Institute of Particle Physics (IPP), Canada
[ad] Also at Institute of Physics and Technology, Ulaanbaatar, Mongolia
[ae] Also at Institute of Physics, Azerbaijan Academy of Sciences, Baku, Azerbaijan
[af] Also at Institute of Theoretical Physics, Ilia State University, Tbilisi, Georgia
[ag] Also at IRFU, CEA, Université Paris-Saclay, Gif-sur-Yvette, France
[ah] Also at L2IT, Université de Toulouse, CNRS/IN2P3, UPS, Toulouse, France
[ai] Also at Lawrence Livermore National Laboratory, Livermore, USA
[aj] Also at National Institute of Physics, University of the Philippines , Diliman, Philippines
[ak] Also at School of Physics and Astronomy, University of Birmingham, Birmingham, UK
[al] Also at Technical University of Munich, Munich, Germany
[am] Also at The Collaborative Innovation Center of Quantum Matter (CICQM), Beijing, China
[an] Also at TRIUMF, Vancouver, BC, Canada
[ao] Also at Università di Napoli Parthenope, Naples, Italy
[ap] Also at Department of Physics, University of Colorado Boulder, Colorado, USA
[aq] Also at Washington College, Chestertown, MD, USA
[ar] Also at Physics Department, Yeditepe University, Istanbul, Türkiye
* Deceased